EFFECTS OF TOTAL SHOULDER ARTHROPLASTY ON GLENOHUMERAL KINEMATICS AND MECHANICS

A Dissertation

Presented to the Faculty of the Graduate School

of Cornell University

in Partial Fulfillment of the Requirements for the Degree of

Doctor of Philosophy

by

Radhika Jayesh Patel

May 2014

EFFECTS OF TOTAL SHOULDER ARTHROPLASTY ON GLENOHUMERAL KINEMATICS AND MECHANICS

Radhika Jayesh Patel, Ph. D.

Cornell University 2014

Glenoid component loosening is the primary reason for failure after a total shoulder arthroplasty (TSA) accounting for 32% of complications post-surgery. The design of the glenoid implant, specifically the degree of conformity or radial mismatch between the bearing surface of the glenoid and humeral components, allows for posterior translation and has been shown to affect glenoid loosening. Existing theories for the failure mechanism are conflicting, suggesting that failure occurs in the bone, cement, or interface, with no agreement on the mechanism that causes glenoid loosening. The focus of this thesis is to obtain a fundamental understanding of glenohumeral joint translations and load transfer in the bone-implant system after a TSA.

First, we studied the posterior glenohumeral translations observed clinically using a six degree of freedom computational model of the shoulder. We found that posterior translation increased as a function of radial mismatch, and the increase in posterior translation was explained by the increase in force in the infraspinatus muscle.

Secondly, using a finite element model of the healthy scapula, we determined that after a cemented TSA, stress shielding was possible because load bypassed the cancellous bone region and was transferred directly to the stiff cortical bone when the implant pegs were present. Additionally, the cement was more likely to failure during eccentric and high magnitude loading. Finally, using finite element models of an osteoarthritic scapula, we showed that stress shielding and cement failure was more likely in the corrected osteoarthritic glenoid compared to the healthy and retroverted osteoarthritic glenoids during eccentric loading. These findings question the common surgical practice of correcting for glenoid retroversion prior to reconstruction. Furthermore, the reconstructed osteoarthritic glenoid was less sensitive to peg length than the healthy glenoid demonstrating that shorter pegs, requiring less bone resection, may be used in osteoarthritic patients.

BIOGRAPHICAL SKETCH

Radhika Patel was born in Elmira, New York on December 2nd, 1986. Her family loves to travel and moved around for several years from New York to Michigan to France and then back to Michigan. During that time and into her high school years, she developed an interest in traveling, dance, and math and biology. After completing high school, she enrolled at Case Western Reserve University and earned her Bachelor of Science degree in Biomedical Engineering in 2009. While studying in Cleveland, she continued to participate in dance competitions, became involved in biomechanics research, and had the opportunity to travel Asia and Africa. In 2009, she made full circle and returned to beautiful upstate New York to join the doctoral program in Mechanical Engineering at Cornell University. She has since earned her Master of Science degree in Mechanical Engineering in 2012 and received the National Science Foundation Graduate Research Fellowship. In addition to conducting research, she was a teaching assistant in the mechanical engineering department. Radhika also served on the executive board as Secretary for the Engineering Graduate Student Association and worked with other graduate engineering students to organize professional and social events for the College of Engineering. Although research kept her busy, outside of academia, Radhika enjoyed dancing, cooking, and exploring new places. Finally, during the summer of her last year at Cornell in 2013, Radhika accepted a 12 week internship at ExxonMobil's Upstream Research Company in Houston, Texas. She enjoyed seeing the crucial role research played in industry and wanted to be further involved with this process in the future. After defending her PhD at Cornell, she will be joining athenahealth in Boston, Massachusetts to help fix healthcare.

ACKNOWLEDGMENTS

My sincerest gratitude goes out to all of the people who have mentored, supported and believed in me every step of the way during my graduate career. I would first like to thank my advisor, Dr. Yingxin Gao, for supporting me through several formulations of my "story." While always there to provide guidance, she also gave me the freedom to create my own research path, which challenged me to think independently and creatively. Thank you for sharing your insight and advice, and for always encouraging me to stay positive. My committee members have also been wonderful mentors throughout the PhD process. Thank you to Timothy Wright and Christopher Hernandez for sharing not only your scientific know-how but also your support over the past several years. I am honored to have worked with all of you and appreciate your assistance.

Successful research cannot be undertaken independently, and my project would not have been completed without the tremendous support of past and present members of the Gao Lab Group, the Biomechanics Department at the Hospital for Special Surgery, and Kirk Gunsallus for all his help with the finite element method and troubleshooting. Also big thank you to Marcia Sawyer and Judy Thoroughman for making many of the logistical graduate school processes go much more smoothly.

During my five years at Cornell, a great amount of support was given to me outside of the lab-thank you to my wonderful friends for all the nights out in downtown, the coffee breaks, dinner dates, vent sessions, and all of the unforgettable memories! I would also like to thank my friends from Case Western and Michigan for their unwavering love, support and patience; I am

truly lucky to have all of you in my life.

Finally, I extend my heartfelt appreciation to my family for their love and always encouraging me to dream big. Thank you to my parents for giving me a strong foundation upon which to grow and for always believing in me through ups and downs. I appreciate your visits to Ithaca, as well as, the many care packages that always brought a smile to my face. Janki, you're an amazing sister, thank you for all your support in all aspects of my life—so glad you're navigating the PhD process with me. Lastly, thank you to Ankit, for being my biggest fan and pushing me to be my best. Your love and support has meant the world to me.

TABLE OF CONTENTS

LIST OF FIGURES

Chapter 1

Chapter 2

Chapter 3

Chapter 4

Chapter 1

Introduction

Osteoarthritis (OA), described as a wear and tear disease, affects some 27 million Americans.[8] Populations over the age of 40 usually begin to develop OA, and those over 65 years of age are considered at high risk for OA.[26] OA can cause pain and loss of function of the joint; significantly affecting the daily activities of living. In 2003, the cost to the healthcare industry was about 128 billion dollars.[27] Joints typically affected with OA are the knees, hips, and shoulders. Following the hip and the knee, the shoulder is the third most common joint affected by osteoarthritis.[25] When conservative treatments are ineffective, a total shoulder arthroplasty (TSA) is the main solution to relieve pain and restore function for the patient. The TSA resurfaces the glenohumeral joint with artificial components. Over 60,000 total shoulder arthroplasties are conducted each year in the US.[24]

The post-operative complication rate is as high as 14.7%, and glenoid component loosening is the most common complication.[1] Previous experimental and computational studies have proposed conflicting failure mechanisms, suggesting that failure occurs in the bone, cement, or interface.[10,11,13,18,23] It is essential to establish an understanding of the kinematics and mechanics of the reconstructed glenohumeral joint to explain clinical observations of glenoid loosening. In order to understand the effects of shoulder reconstruction and associated complications, knowledge of the native anatomy is required.

1.1 The Natural Glenohumeral Joint

The shoulder consists of four joints, and this thesis focused on the glenohumeral joint, which is the articulation of the humeral head and the glenoid (as shown in Fig 1.1A). The glenohumeral joint can be described as a golf ball balancing on a tee, where the humeral head may be approximated as the golf ball and the glenoid as the tee. If the glenoid and humeral head are approximated as spherical surfaces, then the radius of the glenoid is larger than the humeral head, and the surface area of the glenoid is much smaller than the humeral head (Fig 1.1). The glenoid is a shallow surface that neither fully constrains nor conforms to the humeral head. The glenoid contour is pear-shaped and asymmetrical so that the superior portion is narrow and the inferior portion is broad.[21] Due to this unique geometry, the glenohumeral joint has very little bony constraint. The glenohumeral joint has the largest range of motion of all the diarthroidal joints in the body due to its six degree of freedom nature.[9] Because the glenohumeral joint is unconforming and unconstraining, the humeral head is able to translate as well as rotate on the glenoid surface during shoulder motion.

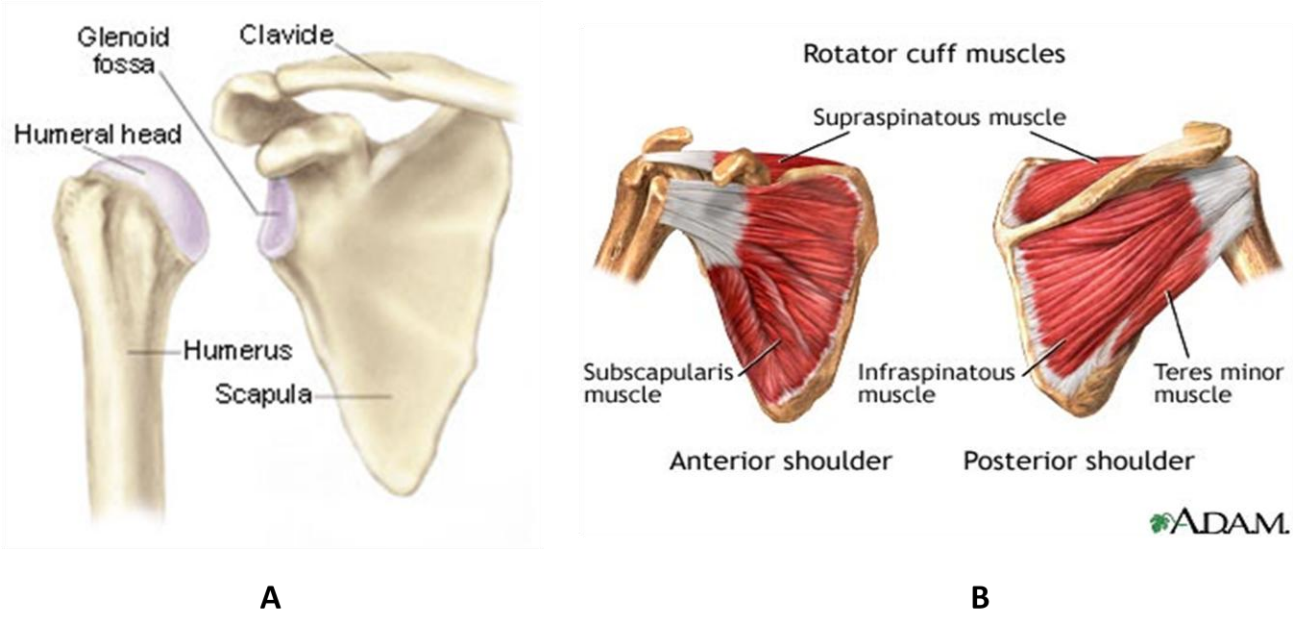

Figure 1.1 A) Glenohumeral anatomy depicting the humerus and humeral head and the scapula and glenoid. Image adapted from http://www.shoulderandlbowcenter.com. B) Rotator cuff muscles crossing the glenohumeral joint. The supraspinatus, infraspinatus, subscapularis and teres minor are shown. Image adapted from A.D.A.M medical encyclopedia.

Stability is maintained in the joint by balancing of the rotator cuff muscles surrounding the joint, the joint capsule and ligaments, and the articulating cartilage. The rotator cuff muscles are a set of four muscles that actively balance and contract to compress and center the humeral head within the boundaries of the glenoid during motion (Fig. 1.1B). The supraspinatus, infraspinatus, subscapularis and teres minor make up the rotator cuff muscles. They each have different lines of action and when activated are coordinated such that in the healthy joint, the humeral head should not dislocate. The ligaments and joint capsule are effective stabilizers during extreme motions of the shoulder when they are stretched beyond their rest length.[20] The main ligaments of the glenohumeral joint include the coracohumeral ligament, and the inferior, superior and middle glenohumeral ligaments as shown in Figure 1.2.[20]

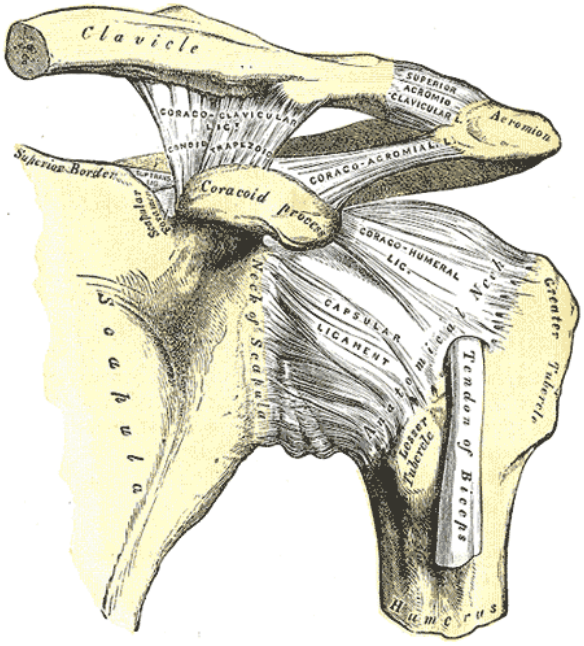

Figure 1.2 Ligaments crossing the glenohumeral joint including the coracohumeral ligament, and the glenohumeral ligaments. Image adapted from Gray's Anatomy, Elsevier, 2008.

Additional stability is given by a layer of articular cartilage on the glenoid and humeral surfaces, which creates a more conforming geometry between the glenoid and humeral head. Furthermore, the compliant nature of cartilage allows the humeral head to translate to the outer edge of the glenoid, and it acts like a shock absorber. There is a delicate balance between anatomy, function, and stability in the natural joint.

1.2 Glenohumeral Osteoarthritis

OA is an age related disease that is associated with wear and tear or abnormal loading of the joint, which causes degeneration of the articular cartilage resulting in pain and loss of function for the patient (Fig. 1.3).

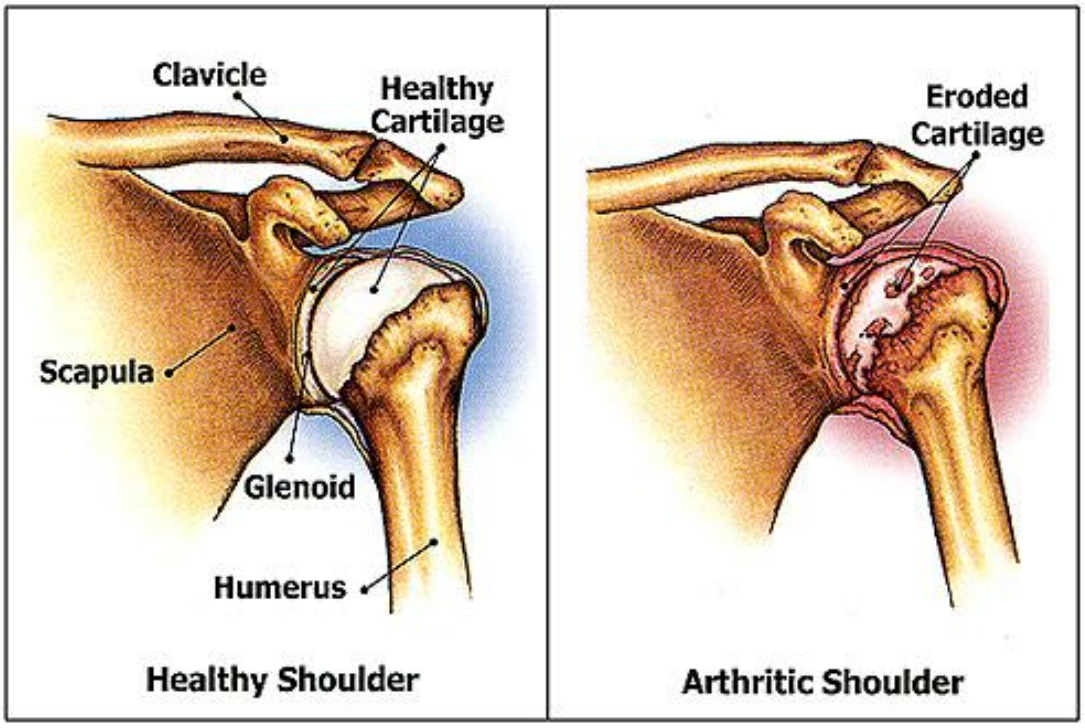

Figure 1.3 Healthy glenohumeral joint with a healthy cartilage lining compared to the osteoarthritic joint with worn cartilage on the glenoid and humeral surfaces. Image adapted from www.orthoteam.com.

In addition to deterioration of the cartilage layer, OA incurs distinctive changes to the bone density and geometry of the glenoid. The bone density of the OA glenoid is higher compared to healthy glenoids.[4] The subchondral bone and cancellous bone regions are shown to stiffen, and spatial changes in bone density are such that the posterior region is stiffer than the anterior region and the inferior region is stiffer than the middle and superior regions of the glenoid.[4] Another change associated with OA is increased posterior glenoid wear leading to a retroverted glenoid. A highly retroverted glenoid can cause increased posterior loading and instability.[3] The angle of glenoid retroversion is calculated by using a superior view of the scapula and drawing a straight line along the length of the scapular spine to the glenoid face (Fig. 1.4).[7] A perpendicular line is drawn to that line, and another line is drawn connecting the posterior edge to the anterior edge

(Fig. 1.4). The resulting angle between these two lines is the angle of glenoid retroversion. Higher angles indicate increased posterior wear.

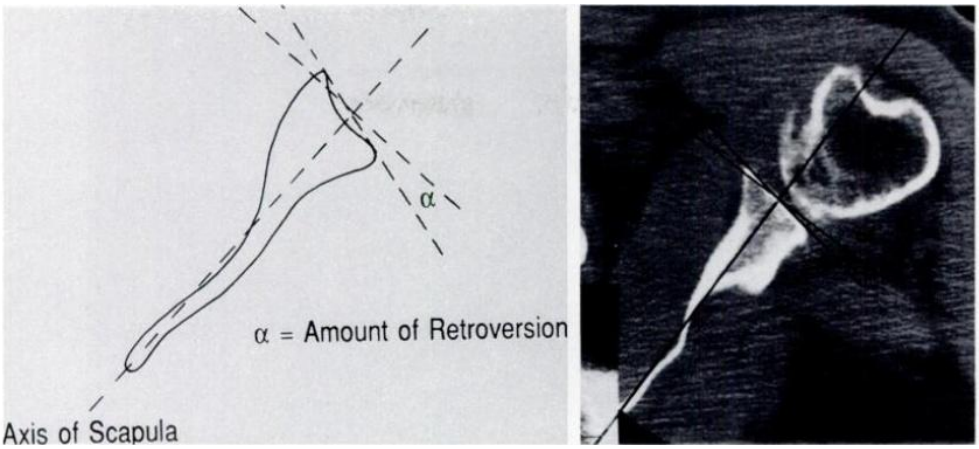

Figure 1.4 Method to determine the amount of retroversion of the glenoid, α. Image adapted from literature (Friedman et al, 1992)

Surgical technique currently aims to correct the retroversion by reaming the anterior portion of the glenoid in order to reduce eccentric loading (and thus mitigate the effects of rocking horse which is attributed to glenoid component loosening).[5,14]

1.3 The Total Shoulder Arthroplasty

A total shoulder arthroplasty (TSA) is the main solution for shoulders afflicted with OA when conservative methods are ineffective. The TSA typically consists of replacing the humeral head and glenoid surfaces with artificial surfaces that mimic the natural geometry (Fig. 1.5). The goal is to relieve pain and reinstate function of the shoulder joint.

Figure 1.5 Typical total shoulder replacements on the market. A polyethylene and pegged glenoid component is typically fixed to glenoid bone with a cement layer. The humeral component is metallic and the metal post is fixed in the humerus with a layer of cement. Image adapted from Zimmer, Inc.

The TSA was originally designed by Pean in 1893 then modernized by Neer in the 1950's.[1] Neer performed a hemiarthroplasty, where only the humeral head was resurfaced, then in 1974 introduced the polyethylene glenoid component. The TSA is only 40 years old, and only slight modifications have been made to the original design since conception.[3] Typically, the humeral head is replaced with a metallic spherical head and stem. The glenoid is implanted with a polyethylene component. The glenoid component comes in many sizes to accommodate individual patient sizes, and differing radial mismatches between the humeral and glenoid components. The orthopaedic device industry has also developed several designs of the glenoid implant; ranging from keeled to pegged and cemented to metal-backed (Fig. 1.6).

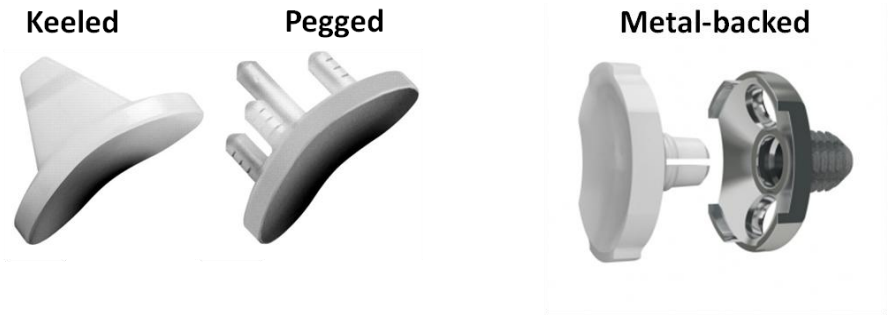

Figure 1.6 Various glenoid components available on the market. Keeled and pegged all-polyetheylene components are fixed in the glenoid with a layer of cement. The polyethylene metal-backed components rely on bony-ingrowth for fixation. Image adapted from Lima Corporate.

The goal of a TSA is to relieve pain and restore function of the shoulder joint. The contemporary TSA relies on the natural balance of the rotator cuff muscles to maintain joint stability. However, due to the six degree of freedom nature of the glenohumeral joint, this task has proved more difficult than in other joints. High complication rates in the mid to long term post-operatively make it clear that the current designs of TSA must be improved to better achieve this goal.[1,22]

1.4 Complications Associated with Total Shoulder Arthroplasty

Complication rates post-operatively have been reported between 12 and 14.7%.[1] Glenoid loosening is the most common complication after a TSA and accounts for a third of the complications post-operatively. The cumulative glenoid loosening rate is as high as 44% 9 years post-operatively.[19] The "rocking horse" phenomenon has been attributed to glenoid component loosening.[6] This phenomenon suggests that eccentric loading on one side of the glenoid component causes compressive stresses at the fixation on that side, and tensile stresses on the opposing side leading to implant loosening (Fig. 1.7).[6,22]

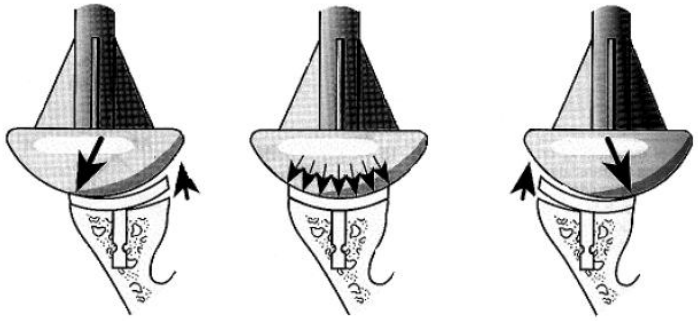

Figure 1.7 Superior view of the reconstructed glenohumeral joint depicting the rocking horse phenomenon due to eccentric loading on the glenoid component. The central image depicts the joint load during center loading, and the images on to the right and left show how application of the joint load is altered with eccentric translation of the humeral head. Eccentric load applied to one side of the implant causes tensile stresses on the opposing side at the fixation surface contributing to glenoid loosening. Image adapted from www.orthop.washington.edu.

Glenoid loosening can cause pain and discomfort such that a revision may even be required. The volume of bone stock available for fixation in the glenoid is minimal which complicates the TSA and makes a revision surgery even more risky. Fixation between the implant and bone is important and ideally must remain secure even during eccentric loading that is common in the glenohumeral joint. Due to the high loosening rates seen post-operatively, fixation is still an issue, however the mechanism for failure is still not understood.[10,11,13,18,23]

Several implant designs have been created over the years aimed to improve fixation between the implant and bone. There are pegged and keeled components that are inserted in the bone.[15] Studies have shown higher radiolucency scores, worse cementing technique, and incomplete seating among patients with keeled compared with pegged components.[12] Cemented glenoid implants require a layer of cement for fixation between the back of the glenoid implant and the implant pegs and the glenoid bone. Metal-backed glenoid components rely on screws to fix into the bone initially then rely on bony-ingrowth as fixation in the long-term.[16,17] Mid-term

results of the metal-backed components are unfavorable with substantial issues related to progression of radiolucent lines and severe osteolysis. There is an increased risk of loosening with metal-backed compared to cemented components; a study found 20% of metal-backed components loosened at three year follow-up compared to 0% with the cemented components.[2] The cemented and pegged implants have proven to be more successful over other designs, however the reported rate of radiolucencies is still high ranging between 36 and 83%.[15,23]

1.5 Research Objectives

Before refining the glenoid implant designs and attempting to decrease the rates of glenoid loosening, it is important to understand how the basic mechanics and kinematics of the joint are affected after a TSA. The overall research objective of this thesis was to obtain a fundamental understanding of glenohumeral joint kinematics and load transfer in the bone-implant system after a TSA. This objective was addressed through the use of a six degree of freedom computational model of the glenohumeral joint and finite element models of healthy and arthritic scapulas.

1.5.1 Nonconforming Glenoid Increases Posterior Glenohumeral Translation after a Total Shoulder Replacement

Our first objective was to explain the posterior glenohumeral translations observed clinically. We hypothesized that the posterior direction of glenohumeral translation during scaption (i.e. elevation in the scapular plane) is related to the radial mismatch. We also hypothesized that the joint contact force would increase as the radial mismatch increased.

1.5.2 Load Transfer after Cemented Total Shoulder Arthroplasty

Our second objective was to gain an understanding of the load transfer through the glenoid before and after reconstruction. Our aim was to determine how load transfer and stress distribution were affected by the introduction of a contemporary glenoid implant, by physiological alterations in the location and magnitude of the joint load on the glenoid, and by the presence of a metal-backing.

1.5.3 Load Transfer after Cemented Total Shoulder Arthroplasty in the Osteoarthritic Glenoid

The objective of this study was to understand the effects of OA induced changes in bone density and retroversion angle of the scapula on load transfer and stress distribution in the bone-implant system of the scapula. Two research questions were addressed: (1) how does the implant peg proximity to the cortical shell affect the load transfer pattern in healthy and osteoarthritic scapulas; (2) how will the local stress distributions and load transfer be affected among the healthy, retroverted osteoarthritic, and corrected osteoarthritic scapulas with center and eccentric joint load?

1.6 Chapter Overviews

To accomplish these aims a deeper understanding of the kinematics and mechanics of the reconstructed glenohumeral joint are required. The goals and complications of a total shoulder arthroplasty and the distinct changes of the osteoarthritic glenoid are introduced as background of this thesis in Chapter 1.

Chapter 2 will describe the six degree of freedom computational model of the shoulder joint used to explain clinical observations of posterior translation. The model took inputs of glenohumeral geometry, used a physiological optimization criterion to determine the necessary muscle forces required to maintain contact between the humeral head and glenoid surfaces while reaching the scaption angle of interest, and output the resulting joint contact force magnitude and location. This study determined the muscle forces and joint contact force magnitude and location for various radial mismatches at different scaption angles. The translation of the humeral head on the glenoid for various radial mismatches gave insight to the in vivo loading conditions and could then be compared to clinical observations of translation. Additionally the muscles that were activated helped to explain the clinical observations of translation.

Chapter 3 goes on to understand how loading conditions affect the stresses in the healthy bone-implant system. A finite element model was developed to understand how the joint load applied at the surface of the implant was carried through the bone-implant system. A metal-backed glenoid component was also simulated to understand the effects of a more stiff material on fixation. This study determined how load was transferred from the implant to the bone and how this load transfer was altered from the healthy glenoid.

Chapter 4 incorporates the effects of the osteoarthritic glenoid after a TSA during eccentric loading. We developed finite element models of both a healthy and osteoarthritic reconstructed scapula implanted with a contemporary glenoid component. Stress distributions in the bone-implant system, and load carried by cement, implant and bone were determined and compared among the shoulder models.

Finally, Chapter 5 summarizes the important conclusions and presents directions for future work.

REFERENCES

1. Bohsali KI, Wirth MA, Rockwood CA. Complications of total shoulder arthroplasty. J Bone Joint Surg. 2006;88(10):2279–92. doi:10.2106/JBJS.F.00125

2. Boileau P, Avidor C, Krishnan SG, Walch G, Kempf J-F, Molé D. Cemented polyethylene versus uncemented metal-backed glenoid components in total shoulder arthroplasty: a prospective, double-blind, randomized study. J Shoulder Elbow Surg. 2002;11(4):351–9. doi:10.1067/mse.2002.125807

3. Brems J. The glenoid component in total shoulder arthroplasty. J Shoulder Elbow Surg. 1993;2(1):47–54. doi:10.1016/S1058-2746(09)80138-9

4. Couteau B, Mansat P, Mansat M, Darmana R, Egan J. In vivo characterization of glenoid with use of computed tomography. J Shoulder Elbow Surg. 2001;10(2):116–22. doi:10.1067/mse.2001.112884

5. Farron A, Terrier A, Büchler P. Risks of loosening of a prosthetic glenoid implanted in retroversion. J Shoulder Elbow Surg. 15(4):521–6. doi:10.1016/j.jse.2005.10.003

6. Franklin JL, Barrett WP, Jackins SE, Matsen FA. Glenoid loosening in total shoulder arthroplasty. Association with rotator cuff deficiency. J Arthroplasty. 1988;3(1):39–46.

7. Friedman RJ, Hawthorne KB, Genez BM. The use of computerized tomography in the measurement of glenoid version. J Bone Joint Surg Am. 1992;74:1032–1037.

8. Helmick, C., Felson, D., Lawrence, R., Gabriel S. Estimates of the Prevalence of Arthritis and Other Rheumatic conditions in the United. Arthritis & Rheumatism. 2008;58(1):15–25.

9. Jobe C, Coen M. Gross Anatomy of the Shoulder. In: Rowe C, editor. The shoulder. New York: Churchhill Livingstone; 1988. p. 38.

10. Junaid S, Gupta S, Sanghavi S, Anglin C, Roger E, Amis A, et al. Failure mechanism of the all-polyethylene glenoid implant. J Biomech. 2010;43(4):714–9. doi:10.1016/j.jbiomech.2009.10.019

11. Lacroix D, Murphy LA, Prendergast PJ. Three-dimensional finite element analysis of glenoid replacement prostheses: a comparison of keeled and pegged anchorage systems. J Biomech Eng. 2000;122(4):430–6.

12. Lazarus MD, Jensen KL, Southworth C, Matsen F a. The radiographic evaluation of keeled and pegged glenoid component insertion. J Bone Joint Surg Am. 2002;84-A(7):1174–82.

13. Mansat P, Briot J, Mansat M, Swider P. Evaluation of the glenoid implant survival using a biomechanical finite element analysis: influence of the implant design, bone properties, and loading location. J Shoulder Elbow Surg. 2007;16(3):S79–S83. doi:10.1016/j.jse.2005.11.010

14. Nowak DD, Bahu MJ, Gardner TR, Dyrszka MD, Levine WN, Bigliani LU, et al. Simulation of surgical glenoid resurfacing using three-dimensional computed tomography of the arthritic glenohumeral joint: the amount of glenoid retroversion that can be corrected. J Shoulder Elbow Surg. 2009;18(5):680–8. doi:10.1016/j.jse.2009.03.019

15. Nuttall D, Haines JF, Trail II. A study of the micromovement of pegged and keeled glenoid components compared using radiostereometric analysis. J Shoulder Elbow Surg. 2004;16(3):S65–70. doi:10.1016/j.jse.2006.01.015

16. Tammachote N, Sperling JW, Vathana T, Cofield RH, Harmsen WS, Schleck CD. Long-term results of cemented metal-backed glenoid components for osteoarthritis of the shoulder. J Bone Joint Surg Am. 2009;91(1):160–6. doi:10.2106/JBJS.F.01613

17. Taunton MJ, McIntosh AL, Sperling JW, Cofield RH. Total shoulder arthroplasty with a metal-backed, bone-ingrowth glenoid component. Medium to long-term results. J Bone Joint Surg Am. 2008;90(10):2180–8. doi:10.2106/JBJS.G.00966

18. Terrier A, Büchler P, Farron A. Bone-cement interface of the glenoid component: stress analysis for varying cement thickness. Clin Biomech. 2005;20(7):710–7. doi:10.1016/j.clinbiomech.2005.03.010

19. Torchia E, Cofield RH, Settergren CR. Total shoulder arthroplasty with Neer prosthesis: Long-term results. J Shoulder Elbow Surg. 1997;6(6):495–505.

20. Veeger HEJ, van der Helm FCT. Shoulder function: the perfect compromise between mobility and stability. J Biomech. 2007;40(10):2119–29. doi:10.1016/j.jbiomech.2006.10.016

21. Williams GR, Abboud JA. Total shoulder arthroplasty : Glenoid component design. J Shoulder Elbow Surg. 2005;14(1S):122–128. doi:10.1016/j.jse.2005.09.028

22. Wirth MA, Rockwood CA. Current Concepts Review - Complications of Total Current Concepts Review Complications of Total Shoulder-Replacement Arthroplasty. J Bone Joint Surg Am. 1996;78(4):603–16.

23. Yian EH, Werner CML, Nyffeler RW, Pfirrmann CW, Ramappa A, Sukthankar A, et al. Radiographic and computed tomography analysis of cemented pegged polyethylene glenoid components in total shoulder replacement. J Bone Joint Surg Am. 2005;87(9):1928–36. doi:10.2106/JBJS.D.02675

24. US Markets for Small Joint Devices. Toronto: Millennium Research Group [Internet]. 2007;Available from: http://www.depuy.com/patients-and-caregivers/shoulder/shoulder-replacement

25. Arthroscopy Association of North America. Joint Replacement Surgery [Internet]. 2009;Available from: http://www.aana.org/EducationLibrary/Articles/JointReplacementSurgery/tabid/128/Default.aspx

26. Centers for Disease Control and Prevention. Arthritis: Osteoarthritis [Internet]. 2011;Available from: http://www.cdc.gov/arthritis/basics/osteoarthritis.htm

27. Centers for Disease Control and Prevention. Arthritis: Arthritis-Related Statistics [Internet]. 2014;Available from: http://www.cdc.gov/arthritis/data_statistics/arthritis_related_stats.htm

Chapter 2

Nonconforming Glenoid Increases Posterior Glenohumeral Translation after a Total Shoulder Replacement[1]

2.1 Introduction

The major complication in total shoulder arthroplasty (TSA) is glenoid loosening, followed by glenohumeral instability with associated complication rates as high as 14.7% within 12 years.[5,36] The design of the glenoid implant, specifically the degree of conformity or radial mismatch between the bearing surface of the glenoid and humeral components, has been shown to affect glenoid loosening.[35] Walch et al demonstrated that a glenohumeral prosthetic mismatch significantly influences the scores for glenoid radiolucent lines.[35] The muscles surrounding the glenohumeral joint play an important role in compressing the humeral head to the glenoid socket. Failure to do so results in humeral translation and therefore eccentric loading on the glenoid. The "rocking horse" phenomenon induced by eccentric loading is commonly attributed to loosening

[1] Patel R, Choi D, Wright T, Gao Y. Nonconforming Glenoid Increases Posterior Glenohumeral Translation after Total Shoulder Replacement. Journal of Shoulder and Elbow Surgery. 2014 (Published)

of the glenoid component as it causes compressive stresses at the fixation surface when the external load is applied at one edge of the glenoid component, and tensile stresses on the opposite end. This phenomenon is indicative of eccentric translation of the humeral head.

Since the natural glenohumeral joint allows the humeral head to translate along the glenoid surface, contemporary TSAs are often designed to be less conforming with a variety of humeral head sizes (depth and radius) and small, medium, and large glenoid sizes.[9] The flexibility provides the surgeon with a range of radial mismatches. Nonetheless, glenoid loosening continues to account for 32% of all TSA complications.[5]

Clinical and implant retrieval studies suggest that radial mismatch allows for humeral head translation posteriorly that may contribute to glenoid loosening.[7,11,15,20,22] A radiographic study showed significant posterior humeral head translation after a TSA when the shoulder was positioned at 90 degrees of abduction across differing angles of flexion.[8] Massimini et al.[20] found significant contact in the superior-posterior quadrant of the glenoid of TSA patients for various angles of abduction using bi-plane fluoroscopy. Retrieved glenoid implants from unconforming TSAs showed consistent patterns of wear and deformation in the postero-superior and postero-inferior quadrants, indicating posterior, inferior, and superior glenohumeral translations.[11,22,23] Although cadaveric and computational studies support that a larger radial mismatch results in greater translations, it is still unclear if the posterior translations observed clinically are induced by the radial mismatch.[2,13,16]

Our objective was to explain the posterior glenohumeral translations observed clinically. We hypothesized that the posterior direction of glenohumeral translation during scaption is related to the radial mismatch. We also hypothesized that the joint contact force would increase as the radial mismatch increased. To prevent dislocation, the muscles in the shoulder would

coordinate in an effort to keep the humerus centered on the glenoid, thus increasing the muscle forces across the joint and increasing the joint contact force. To test our hypotheses, we developed a six degree of freedom computational model to predict joint contact location and magnitude during scaption. The use of a computational model allowed us to perform a sensitivity study of radial mismatch.

2.2 Materials and Methods

We developed a computational model to determine the effect of radial mismatch on glenohumeral translations and joint contact force from 20 to 60 degrees of scaption. The geometrical parameters necessary as inputs to the computational model were obtained from a cadaveric shoulder attached to a shoulder simulator. We tested radial mismatches ranging from 1mm to 20mm, spanning the range available commercially (Comprehensive®, Biomet, Warsaw, IN), by changing the radius of the glenoid surface in the computational model. Muscle forces, joint contact load and glenohumeral head translation were calculated at desired positions to evaluate the effects of radial mismatch.

The computational model consisted of the bearing surfaces of the glenohumeral joint and five muscles that contribute to scaption: deltoid, subscapularis, supraspinatus, infraspinatus, and teres minor. Muscles with larger cross-sectional areas were subdivided to more accurately model the lines of action: the deltoid was divided into anterior, posterior, and middle parts; the subscapularis was divided into superior and inferior parts. The scapular and humeral coordinate frames and all the necessary anatomical landmarks were defined according to recommendations of the International Society of Biomechanics for joint coordinate systems.[37]

To develop the computational model, a shoulder simulator was used to acquire the necessary geometry from a reconstructed cadaver. The simulator experiment was previously described.[10] Briefly, all soft tissues of the left shoulder from a 74 year old male were dissected free of the scapula and humerus, except for the tendinous insertions of the five muscles that were included in our model. A total shoulder replacement was performed by an experienced surgeon using an unconstrained Biomet implant with a 13.1mm radial mismatch; the glenoid radius was 38.1mm and the humeral head radius was 25mm. A medium-sized glenoid component was selected for this specimen. The anatomic glenoid retroversion was not measured, however a healthy specimen was used, and a typical TSR procedure was performed. The retroversion (if any) was corrected. Teflon-coated steel cables were sutured to the tendon insertion sites to represent the muscles. The line of action of the muscle as determined by the surgeon was represented by the path of the cable. The weight of the arm was simulated by a 3.5kg weight located 315 mm from the greater tuberosity to replicate the center of gravity for the entire upper extremity.[27] The scapula was rigidly fixed to the simulator table while the humerus was free to rotate about the glenohumeral joint.

The geometry of the glenohumeral joint was determined by using a motion capture digitizer to determine points of interest: muscle origins and insertions, epicondyles, humeral head center, and glenoid center. The humeral head center was established by tracking markers on the humerus while circulating the humeral head within the glenoid component and then applying a least squares algorithm to the resulting data.

The geometry of the shoulder obtained from the physical setup was used to create a computational model that determined the resulting glenohumeral translations, muscle forces and joint contact force. In our model, we simulated scaption angles ranging from 20 to 60 degrees for

all radial mismatches characterizing the common daily motions during which higher glenohumeral contact forces would be expected. Only glenohumeral motion was modeled because we were primarily interested in force distributions around the glenohumeral joint, and thus scapulothoracic motion was not included. The muscle forces required to maintain the desired scaption angle were determined by an optimization program, in which a physiological cost function was used to predict the muscle forces across the joint by minimizing the sum of the stresses cubed in the muscles: $J = \min \sum_{i=1}^{8} \sigma_i^3$.[6] Muscle stresses were calculated by dividing the muscle force in each muscle by its cross sectional area obtained from literature.[18] The optimized set of muscle forces was required to maintain static equilibrium. Additional constraints included that the muscles remain in tension, that the muscle forces not exceed the maximum force generated by the muscle (specific tension of the muscle times its physiological cross-sectional area), and that the joint contact force vector remain directed within the glenoid surface area.[18]

The glenoid and humeral contact surfaces of the joint were modeled as frictionless, spherical surfaces of differing radii. We assumed that contact of the humeral head occurred normal to the surface of the glenoid, such that the contact vector was coincident with the glenoid center and humeral head center (Fig. 2.1). The translations were determined by calculating the displacement of the humeral head center, which were defined by angles θ and φ, the angles between the joint contact vector and the middle of the glenoid in the transverse and coronal planes, respectively: $x = \rho \sin\theta$; $y = \rho \sin\varphi$; $z = \rho(\cos^2\theta - \sin^2\varphi)^{1/2}$, where x, y, z are the translations of the humeral head and ρ is the radial mismatch. Radial mismatches from 1 to 20 mm were examined including a radial mismatch of 13mm to model the physical implant with 13.1mm radial mismatch. Translations were limited to within the surface area of the glenoid (i.e.

the contact force vector had to be directed within the glenoid implant).[29] Angles, θ_{max} and φ_{max}, defined the 3D spherical surface area of the implant in the anterior /posterior (AP) and superior/inferior (SI) directions, respectively, as represented by the bolded orange region of the circle in Figure 2.1. Angles θ_{max} and φ_{max} were based on the 38.1mm glenoid implant radius and its respective AP and SI dimensions used in the physical simulator experiment. The maximum translation allowed for each radial mismatch was calculated by: $x_{max} = \rho \sin \theta_{max}$;

$y_{max} = \rho \sin \varphi_{max}$; $z_{max} = \rho(\cos^2 \theta_{max} - \sin^2 \varphi_{max})^{1/2}$.

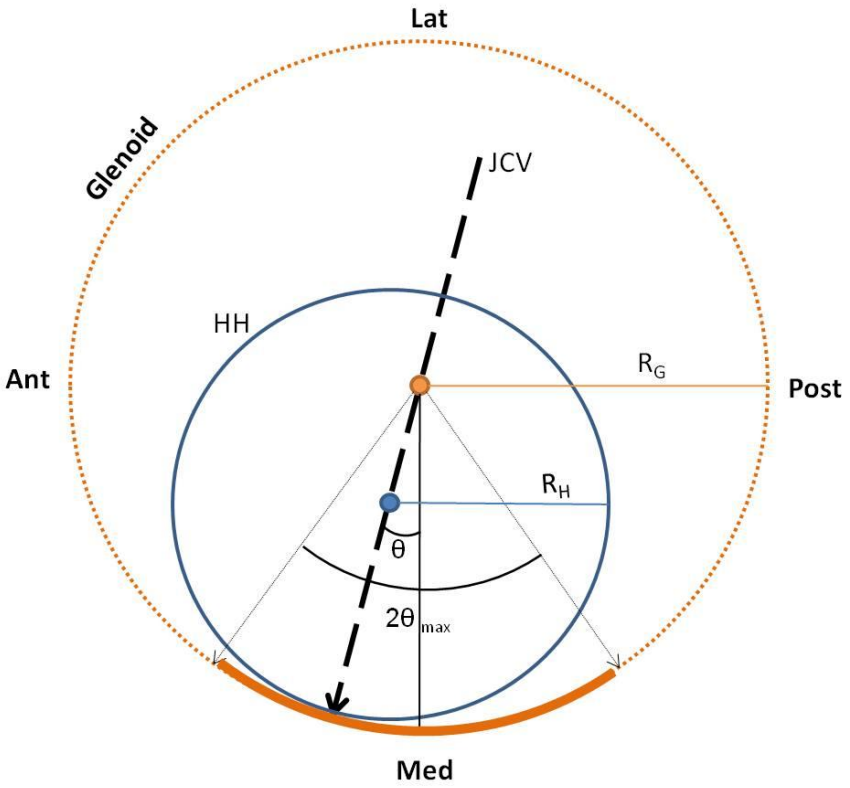

Figure 2.1 Schema of a transverse view of the joint contact vector, JCV, and translation of the humeral head on the glenoid surface. The humeral head, HH, is shown as a blue circle with radius RH and with center shown by a filled blue circle. An axial projection of the glenoid surface with radius RG is shown as the orange arc and its center is shown by a filled orange circle. Contact of the head was assumed to occur normal to the glenoid surface. θ is the angle between the contact vector and the middle of the glenoid. Angle θ_{max} defines the maximum allowable translation in the AP direction. Ant, Post, Sup, and Inf represent anterior, posterior, superior, and inferior, respectively.

Additionally a muscle wrapping algorithm was incorporated to model the physiological path of the muscle from its point of origin to insertion.[3] Anatomically the muscles surrounding the shoulder tend to wrap around the bony architecture of the joint during axial rotation and scaption, which can affect the muscle moment arm.[14] The biomechanical validity of the model was confirmed by comparing the moment arm to those reported in the literature.

2.3 Results

As the radial mismatch increased, the contact location of the humeral head on the glenoid changed. Figure 2.2A shows a representative image of the contact locations for different radial mismatches of the humeral head on the glenoid implant surface. For a radial mismatch of 1mm, the humeral head made contact in the superior and posterior quadrants of the glenoid implant. Although the humeral head stayed within the posterior quadrant as the radial mismatch increased, the contact location moved inferiorly with increasing mismatch. At 10mm of radial mismatch, the head was about 5mm posterior to the glenoid center, and at 20mm of radial mismatch, the head contacted about 7mm posterior and 1mm inferior to the glenoid center. Similar trends occurred for all degrees of scaption; Figure 2.2B shows an expanded view of contact locations for 30 and 60 degrees.

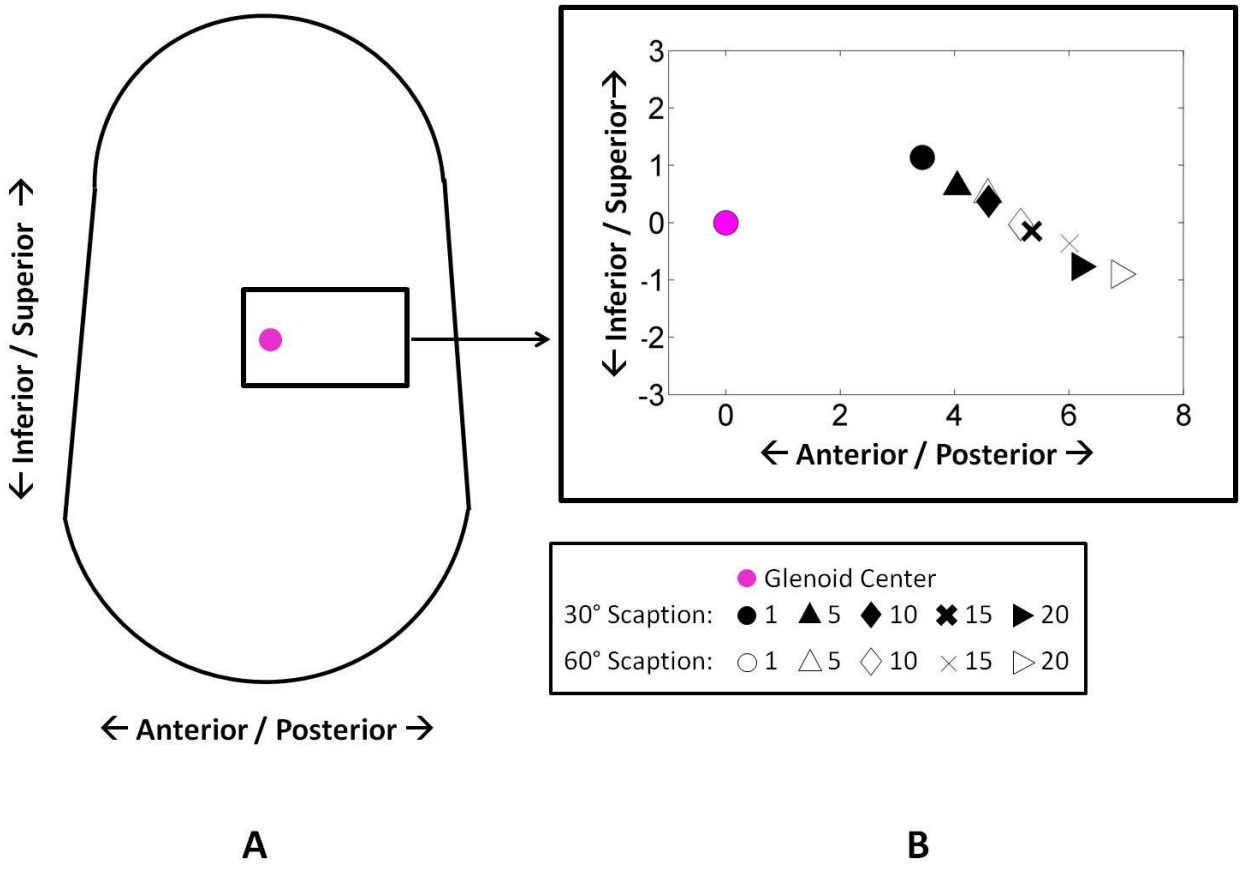

Figure 2.2 A) Representative contour of a lateral view of the glenoid implant with area of interest specified. The pink circle is the glenoid center. B) Enlarged lateral view of the area of interest, where the markers represent values of radial mismatch. Joint contact location markers at 30 degrees (filled markers) and 60 degrees (hollow markers) of scaption for 1 to 20mm of radial mismatch.

Increased humeral head translations were observed with increased radial mismatch (Fig. 2.3). The amount of SI translation increased from 0.04mm superiorly to 0.4mm inferiorly, and AP translation increased from 0.2 to 3.1mm posteriorly from the glenoid center as the radial mismatch increased from 1mm to 20mm.

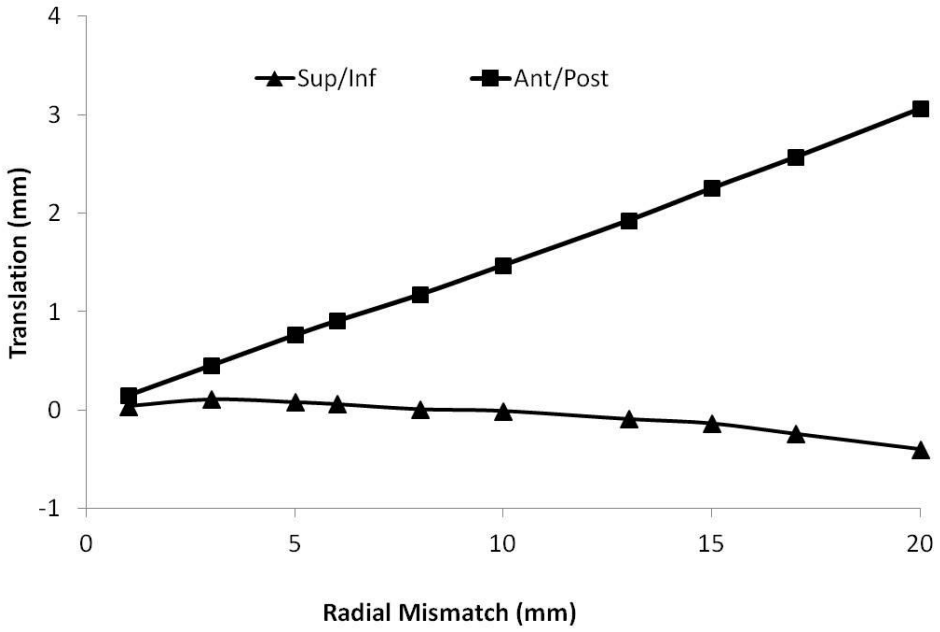

Figure 2.3 Superior and posterior translations of the humeral head as the radial mismatch was varied from 1 to 20mm at 60 degrees of scaption.

The joint contact force increased as the scaption angle increased from 20 to 60 degrees (Fig. 2.4), regardless of the radial mismatch. However, as radial mismatch increased at a given scaption angle, the magnitude of the joint contact force remained relatively constant, since it only increased by 22N over a 19mm increase in radial mismatch (Fig. 2.5). The direction of the contact force was also relatively consistent. The majority of the joint force was compressive, and the ratio of shear to compressive force was 0.1 and remained relatively constant as the radial mismatch increased. This trend was observed for all the scaption angles. The muscle forces changed as the radial mismatch increased. The middle deltoid force decreased by 3% while the supraspinatus and infraspinatus muscle forces increased by 9% and 11%, respectively. All other muscles had negligible changes in force.

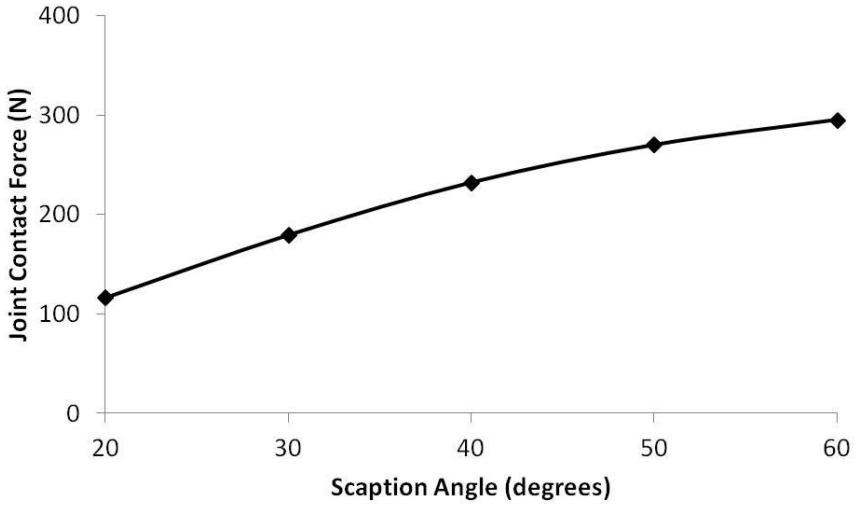

Figure 2.4 Representative trend for the magnitude of the joint contact force as scaption angle increases from 20 to 60 degrees (trend was similar for all radial mismatches, but the one shown is for a radial mismatch of 13mm).

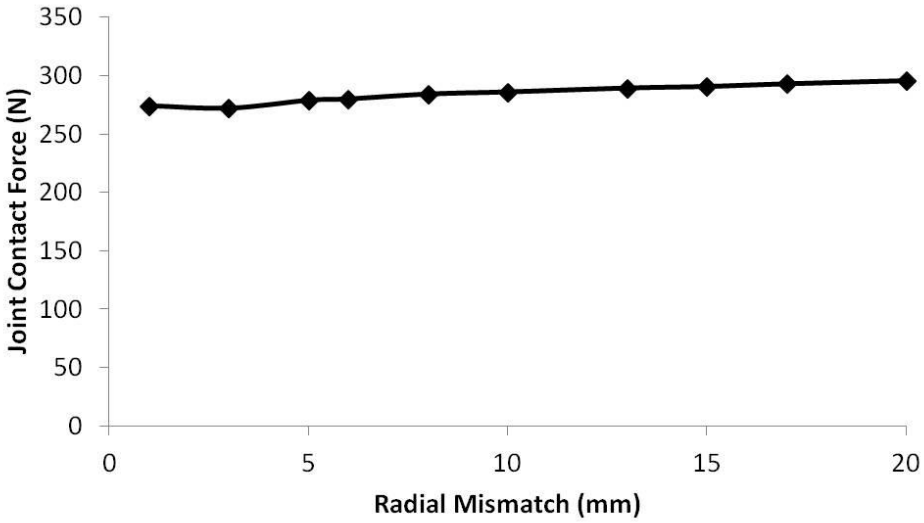

Figure 2.5 Magnitude of glenohumeral joint contact force as the radial mismatch was varied from 1 to 20mm at 60 degrees scaption.

The moment arm values of the middle deltoid, infraspinatus, and supraspinatus are shown in Figure 2.6. The functions of the muscles remained consistent throughout the range of scaption

angles evaluated, i.e. the middle deltoid and supraspinatus were confirmed as abductors and the infraspinatus as an external rotator.

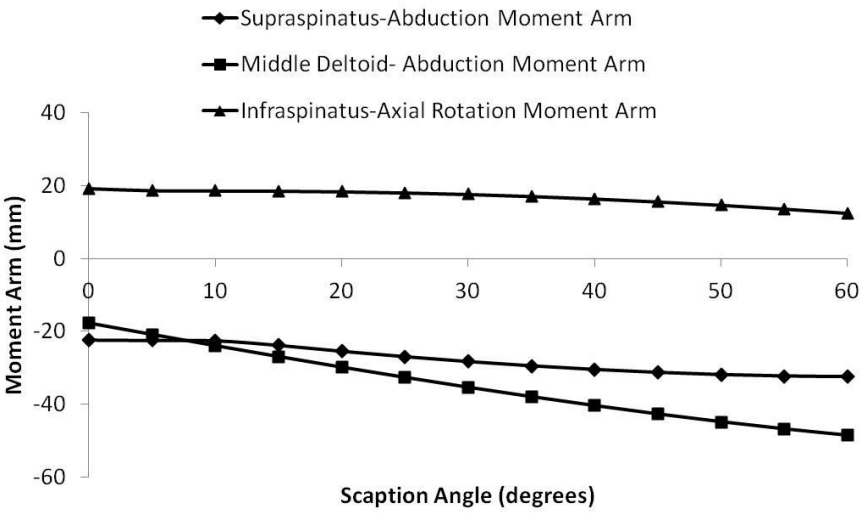

Figure 2.6 Moment arm values for the middle deltoid, supraspinatus and infraspinatus. The moment arms of abduction (negative values represent abduction) for the middle deltoid and supraspinatus are shown. The moment arms of axial rotation (positive values represent external rotation) for the infraspinatus are shown.

2.4 Discussion

The degree of radial mismatch in a total shoulder implant affects glenohumeral joint translations and may affect glenoid loosening. However the effect of radial mismatch on the direction of glenohumeral joint translation, necessary to explain clinical observations of posterior translation has not been investigated previously. We hypothesized that the posterior direction of glenohumeral translation during scaption is related to the radial mismatch. Additionally, we hypothesized that the joint contact force would increase as the radial mismatch increased.

The results from our six degree of freedom computational shoulder model indicated that as the degree of conformity decreased (i.e. the radial mismatch between the humeral head and

the surface of the glenoid component increased), the contact location of the humeral head on the glenoid surface translated more posteriorly and inferiorly. Although the contact location remained in the posterior quadrant as the radial mismatched increased, the translation increased more in the AP direction than in the SI direction, resulting in eccentric posterior loading that has been associated with the "rocking horse" phenomenon that causes loosening and failure of the glenoid component.[7]

The large amount of posterior translation found in our study is commonly observed clinically in both native and reconstructed shoulders. Soslowsky et al.[28] demonstrated posterior glenohumeral contact during scaption in normal cadaver joints with intact ligaments and capsule taken through a large range of motion using simulated rotator cuff and deltoid muscle forces. Patients with osteoarthritis frequently experience asymmetric posterior wear of the glenoid articular cartilage[36], and Walch et al.[34] reported that 32% of patients suffering from osteoarthritis experience posterior subluxation due to asymmetric glenoid cartilage wear.[5] Additionally, Bohsali et al.[5] reported that about 6% of complications after a TSA occur due to posterior instability. For the reconstructed shoulder, in vivo imaging, implant retrieval studies, and radiographs all demonstrate significant posterior and superior translation of the humeral head.[8,11,20,22,23,32] These clinical findings and our results serve to emphasize the importance of joint conformity in both the normal and reconstructed shoulder.

The posterior translations determined by our model can be attributed to the collaborative effect of the middle deltoid and the rotator cuff muscle forces. The stabilizing mechanisms of the glenohumeral joint are provided by the deltoid and rotator cuff muscles, the glenohumeral ligaments and capsule, and the joint contact load. The ligament and capsule only stretch to constrain the joint with extreme rotations.[33] A general trend in muscle forces suggested that as

the radial mismatch increased, the force of the abducting middle deltoid decreased and the forces of the rotator cuff muscles increased, specifically for the supraspinatus and the infraspinatus. It is well-recognized that the rotator cuff muscles serve as stabilizers in the natural shoulder by compressing the humeral head into the glenoid socket; the infraspinatus and subscapularis form a medially directed transverse couple, and the supraspinatus compresses the glenoid to prevent superior humeral head translation.[14] The middle deltoid has a superiorly directed line of action, so activation of this muscle causes superior translation of the humeral head.[14] As the radial mismatch increases, the humeral head can translate more, but in an effort to stabilize the joint, our model reduced the superiorly directed force in the middle deltoid and increased the stabilizing forces of the infraspinatus and supraspinatus. Our model showed that as the infraspinatus force increased so did posterior translation; Pande et al.[26] similarly determined that the humeral head can be pulled posteriorly due to activation of the infraspinatus muscle. This finding is important in rehabilitation after TSA. Because the subscapularis muscle provides resistance against posterior humeral head translation, a subscapularis muscle weakened by surgery should be post-operatively strengthen to decrease the chances of posterior instability.[4,21]

The joint contact force magnitude and direction at the glenohumeral joint remained relatively insensitive to radial mismatch. The slight changes in joint contact force can be attributed to the balancing effects of the glenohumeral muscles. Although a redistribution of muscle forces was observed, the overall effect of these changes did not markedly affect the contact force. The contact force magnitudes in our study were lower than those measured *in vivo* by Nikooyan et al.[24] (290N versus 450N); however, the trend of increasing contact force as scaption angle increases agrees well with their findings. This model simulated the muscle lines of action for five muscles; however, additional muscles that that also play a role in glenohumeral

movement were not included in this study. If the number of muscles were increased in this study, we might expect an increase in the total joint reaction force. Furthermore, our computational model represented the joint contact force vector as a single point of application, so even though the magnitude did not vary, the stresses in the glenoid component, fixation interfaces, and surrounding bone could all increase, because as radial mismatch increases, the surface area of contact decreases.[30]

Our model showed that the posterior glenohumeral translations were linearly related to radial mismatch (R^2 = 0.999 in SI and R^2=0.869 in AP translation), which agrees with previously reported findings.[13,16] However our finding that the joint contact location was positioned in the posterior quadrant does not agree with Terrier et al.[30], who suggested the joint contact location remained centered within the glenoid component even with varying radial mismatch. But Terrier et al. included only three muscle forces, and these muscles responded passively to external load. Our model was more comprehensive since we modeled five muscles that were considered active structures controlling the position.

In general, reasonable agreement existed between our moment arm values and the range of values found in the literature. Our study supports that the teres minor and the infraspinatus act as external rotators.[18,25] Internal rotation of the inferior and superior subscapularis matched well with the range of moment arms in the study by Otis et al.[25] Moment arms of abduction for the anterior and posterior deltoids as well as the inferior and superior subscapularis also agreed with values reported in the literature.[1,12,17,25] The abduction moment arm of the middle deltoid was slightly larger than that reported in the literature, but this is likely due to our shoulder simulator in which origins of the deltoid muscles were slightly raised by vertically-adjustable overhead pulleys to prevent wrapping around the acromion.[12,17,18,25] The pulleys were a method to more

accurately model the lines of action of the deltoid. The current computational model includes a muscle wrapping algorithm to more accurately model the lines of action of rotator cuff muscles that wrap around the humeral head. As the deltoid wraps around other bony structures, instead of the humeral head, it is too complicated to include in the current model. Therefore the three lines of action of the deltoid were modeled more accurately as a straight lines starting from its insertion on the humerus to the pulleys, which were assumed to be the location where wrapping occurs. The larger deltoid moment arms could also account for the lower joint contact force magnitude observed in our study.

The advantage of our computational model is the ability to predict both rotation and translation of the glenohumeral joint. Previous numerical models of the glenohumeral joint do not include glenohumeral translation. To our knowledge only one other six degree of freedom model exists that can predict translations during abduction.[31] In this other model, only superior translation was observed, while we found a significant amount of posterior translation. Multiple differences between the models could explain the different results. First, different motions were simulated (abduction vs. scaption). Second, we used optimization of a physiological criterion to determine the muscle forces applied across the joint for a given position, whereas Terrier et al.[31] used ratios of EMG and cross-sectional area to determine given muscle forces. The ultimate translations will be affected by the applied muscle forces.

Our study has limitations. First, we modeled the geometry of only a single cadaveric specimen; however, we found that the moment arms of the cadaver matched well with literature values.[1,12,17,19,25] Second, we did not include soft tissue constraints; however, the range of motion we simulated was within the range where passive tissue constraints are not active.[33] Furthermore, we modeled only eight muscle lines of action due to the physical limitations of our shoulder

simulator; inclusion of more muscles could affect the cost function and estimation of muscle force. Finally, the computational model is currently only capable of modeling spherical geometries for the articulating surfaces, such as in the case of a reconstructed joint, and therefore cannot to model the native joint. Despite these limitations, our model explained clinical observations and provided an understanding of how the degree of radial mismatch affects glenohumeral translations.

2.5 Conclusion

In conclusion, we successfully quantified the effects of radial mismatch on glenohumeral joint translations and joint contact mechanics using a six degree of freedom computational model. We found that increasing radial mismatch affected the humeral head translation by increasing posterior glenohumeral translations. Our results show that clinical observations of posterior translation can be attributed to the balancing forces of the middle deltoid, infraspinatus, and supraspinatus muscles. Additionally, we determined that high radial mismatches (as high as 20mm) may lead to eccentric posterior loading on the glenoid component, which could lead to glenoid loosening and implant failure. We intend to use the contact loads and locations from our current work to determine the load transfer pathways in the TSA bone-implant system through the use of the finite element method.

REFERENCES

1. Ackland DC, Pak P, Richardson M, Pandy MG. Moment arms of the muscles crossing the anatomical shoulder. J Anat. 2008;213(4):383–90. doi:10.1111/j.1469-7580.2008.00965.x

2. Anglin C, Wyss UP, Pichora DR. Shoulder prosthesis subluxation: theory and experiment. J Shoulder Elbow Surg. 2000;9(2):104–14.

3. Audenaert A, Audenaert E. Global optimization method for combined spherical-cylindrical wrapping in musculoskeletal upper limb modelling. Comput methods Programs Biomed. 2008;92(1):8–19. doi:10.1016/j.cmpb.2008.05.005

4. Blasier RB, Soslowsky LJ, Malicky DM, Palmer ML. Posterior Glenohumeral Subluxation : Active and Passive Stabilization in a Biomechanical Model. J Bone Joint Surg Am. 1997;79(3):433–440.

5. Bohsali KI, Wirth MA, Rockwood CA. Complications of total shoulder arthroplasty. J Bone Joint Surg Am. 2006;88(10):2279–92. doi:10.2106/JBJS.F.00125

6. Crowninshield RD, Brand RA. A physiologically based criterion of muscle force prediction in locomotion. J Biomech. 1981;14(11):793–801.

7. Franklin JL, Barrett WP, Jackins SE, Matsen FA. Glenoid loosening in total shoulder arthroplasty. Association with rotator cuff deficiency. J Arthroplasty. 1988;3(1):39–46.

8. Friedman RJ. Glenohumeral translation after total shoulder arthroplasty. J Shoulder Elbow Surg. 1992;1(6):312–316.

9. Graichen H, Hinterwimmer S, von Eisenhart-Rothe R, Vogl T, Englmeier K-H, Eckstein F. Effect of abducting and adducting muscle activity on glenohumeral translation, scapular kinematics and subacromial space width in vivo. J Biomech. 2005;38:755–60. doi:10.1016/j.jbiomech.2004.05.020

10. Gulotta L V, Choi D, Marinello P, Knutson Z, Lipman J, Wright T, et al. Humeral component retroversion in reverse total shoulder arthroplasty: a biomechanical study. J Shoulder Elbow Surg. 2011;21(9):1121–7. doi:10.1016/j.jse.2011.07.027

11. Hertel R, Ballmer FT. Observations on retrieved glenoid components. J Arthroplasty. 2003;18(3):361–6. doi:10.1054/arth.2003.50048

12. Holzbaur KRS, Murray WM, Delp SL. A Model of the Upper Extremity for Simulating Musculoskeletal Surgery and Analyzing Neuromuscular Control. Ann Biomed Eng. 2005;33(6):829–840. doi:10.1007/s10439-005-3320-7

13. Hopkins AR, Hansen UN, Amis AA, Taylor M, Emery RJ. Glenohumeral Kinematics Following Total Shoulder Arthroplasty : A Finite Element Investigation. J Orthop Res. 2007;25(1):108–115. doi:10.1002/jor

14. Jobe CM, Coen MG. Anatomy of the Shoulder. In: Rockwood C, editor. The Shoulder-Volume I. Philadelphia: Saunders; 2004. p. 48–62. (ISBN No. 0-7216-0148-0)

15. Kang RW, Frank RM, Nho SJ, Ghodadra NS, Verma NN, Romeo AA, et al. Complications associated with anterior shoulder instability repair. Arthroscopy. 2009;25(8):909–20. doi:10.1016/j.arthro.2009.03.009

16. Karduna AR, Williams GR, Williams JL, Iannotti JP. Glenohumeral Joint Translations before and after Total Shoulder Arthroplasty. A Study in Cadavera. J Bone Joint Surg Am. 1997;79:1166–74.

17. Kuechle DK, Newman SR, Itoi E, Morrey BF, An KN. Shoulder muscle moment arms during horizontal flexion and elevation. J Shoulder Elbow Surg. 1996;6(5):429–39.

18. Langenderfer J, Jerabek SA, Thangamani VB, Kuhn JE, Hughes RE. Musculoskeletal parameters of muscles crossing the shoulder and elbow and the effect of sarcomere length sample size on estimation of optimal muscle length. Clin Biomech. 2004;19(7):664–70. doi:10.1016/j.clinbiomech.2004.04.009

19. Langenderfer JE, Patthanacharoenphon C, Carpenter JE, Hughes RE, Engineering B, Wright FL. Variation in External Rotation Moment Arms among Subregions of Supraspinatus , Infraspinatus , and Teres Minor Muscles. J Orthop Res. 2006;24(8):1737–1744. doi:10.1002/jor

20. Massimini DF, Li G, Warner JP. Glenohumeral contact kinematics in patients after total shoulder arthroplasty. J Bone Joint Surg Am. 2010;92(4):916–26. doi:10.2106/JBJS.H.01610

21. Miller SL, Hazrati Y, Klepps S, Chiang A, Flatow EL. Loss of subscapularis function after total shoulder replacement: A seldom recognized problem. J Shoulder Elbow Surg. 2003;12(1):29–34. doi:10.1067/mse.2003.128195

22. Nho SJ, Ala OL, Dodson CC, Figgie MP, Wright TM, Craig E V, et al. Comparison of conforming and nonconforming retrieved glenoid components. J Shoulder Elbow Surg. 2008;17(6):914–20. doi:10.1016/j.jse.2008.04.010

23. Nho SJ, Nam D, Ala OL, Craig E V, Warren RF, Wright TM. Observations on retrieved glenoid components from total shoulder arthroplasty. J Shoulder Elbow Surg. 2009;18(3):371–378. doi:10.1016/j.jse.2008.12.006

24. Nikooyan AA, Veeger HEJ, Westerhoff P, Graichen F, Bergmann G, van der Helm FCT. Validation of the Delft Shoulder and Elbow Model using in-vivo glenohumeral joint contact forces. J Biomech. 2010;16;43(15):3007–14. doi:10.1016/j.jbiomech.2010.06.015

25. Otis JC, Jiang CC, Wickiewicz TL, Peterson MG, Warren RF, Santner TJ. Changes in the moment arms of the rotator cuff and deltoid muscles with abduction and rotation. J Bone Joint Surg Am. 1994;76(5):667–676.

26. Pande P, Hawkins R, Peat M. Electromyography in voluntary posterior instability of the shoulder. Am J Sports Med. 1989;17(5):644–8.

27. Poppen NK, Walker PS. Forces at the glenohumeral joint in abduction. Clin Orthop Relat Res. 1978;(135):165–70.

28. Soslowsky LJ, Flatow EL, Bigliani LU, Pawluk RJ, Ateshian GA, Mow VC. Quantitation of in situ contact areas at the glenohumeral joint: a biomechanical study. J Orthop Res. 1992;10(4):524–34. doi:10.1002/jor.1100100407

29. Steenbrink F, de Groot JH, Veeger HEJ, van der Helm FCT, Rozing PM. Glenohumeral stability in simulated rotator cuff tears. J Biomech. 2009;7(11):1740–5. doi:10.1016/j.jbiomech.2009.04.011

30. Terrier A, Büchler P, Farron A. Influence of glenohumeral conformity on glenoid stresses after total shoulder arthroplasty. J Shoulder Elbow Surg. 2006;15(4):515–20. doi:10.1016/j.jse.2005.09.021

31. Terrier A, Reist A, Vogel A, Farron A. Effect of supraspinatus deficiency on humerus translation and glenohumeral contact force during abduction. Clin Biomech (Bristol, Avon). 2007;22(6):645–51. doi:10.1016/j.clinbiomech.2007.01.015

32. Torchia E, Cofield RH, Settergren CR. Total shoulder arthroplasty with Neer prosthesis: Long-term results. J Shoulder Elbow Surg. 1997;6(6):495–505.

33. Veeger HEJ, van der Helm FCT. Shoulder function: the perfect compromise between mobility and stability. J Biomech. 2007;40(10):2119–29. doi:10.1016/j.jbiomech.2006.10.016

34. Walch G, Badet R, Boulahia A, Khoury A. Morphologic study of the glenoid in primary glenohumeral osteoarthritis. J Arthroplasty. 1999;14(6):756–60.

35. Walch G, Edwards TB, Boulahia A, Boileau P, Mole D, Adeleine P. The influence of glenohumeral prosthetic mismatch on glenoid radiolucent lines: results of a multicenter study. J Bone Joint Surg Am. 2002;84-A(12):2186–91.

36. Wirth MA, Rockwood CA. Current Concepts Review - Complications of Total Current Concepts Review Complications of Total Shoulder-Replacement Arthroplasty. J Bone Joint Surg Am. 1996;78(4):603–16.

37. Wu G, Vanderhelm FC, Veeger HEJ, Makhsous M, Van Roy P, Anglin C, et al. ISB recommendation on definitions of joint coordinate systems of various joints for the reporting of human joint motion--Part II: shoulder, elbow, wrist and hand. J Biomech. 2005;38(5):981–992. doi:10.1016/j.jbiomech.2004.05.042

Chapter 3

Load Transfer after Cemented Total Shoulder Arthroplasty[2]

3.1 Introduction

Glenoid loosening is the primary reason for failure after a total shoulder arthroplasty (TSA) accounting for 32% of complications post-surgery.[3,23] The "rocking horse" phenomenon induced by eccentric loading is commonly attributed to loosening of the glenoid component as it causes compressive stresses at the fixation surface when the external load is applied at the superior or inferior edge of the glenoid component, and tensile stresses on the opposite end.[9,23] However, how this phenomenon affects the mechanics of the bone-implant system, and in turn impacts failure, remains unclear. Existing theories are conflicting, suggesting that failure occurs in the bone, cement, or interface, with no agreement on the mechanism that causes glenoid loosening.[14,16,18,22,24]

This lack of consensus is in large part responsible for the broad array of glenoid implant designs that have been developed in an effort to decrease the rate of loosening. Keels and pegs are commonly used as fixation features, and for some designs a metal-backing is incorporated to

---

[2] Patel R, Wright T, Gao Y. Load Transfer after Cemented Total Shoulder Arthroplasty. Journal of Shoulder and Elbow Surgery. 2014 (Published)

supplement fixation between the implant and the bone with or without the use of cement. Non-metal-backed designs have a greater survival rate than metal-backed designs, and pegged designs have a lower incidence of radiolucency than keeled designs.[4,7,19–21] Although better fixation has been suggested with cemented and pegged implants, the rate of radiolucencies is still as high as 36 to 83% in these commonly used designs, consistent with high aseptic loosening rates.[19,24]

While considerable effort has gone into glenoid implant design based on local stress distributions, little understanding exists of the global load transfer patterns that influence local stresses. Previous studies focused on how variables, such as cement mantle thickness, loading position, or implant design, altered the local stresses in the cement, the surrounding bone, or at fixation interfaces.[5,22] Such parametric analyses have the advantage of focusing the effects of each parameter on local stress distributions. However global load redistributions affect the local stresses that lead to failure. Exploring load transfer was successful in developing solutions to early failures in hip and knee replacement by elucidating the factors contributing to implant failure.[1,2,6,12,13,15,17] Finite element (FE) models determined at a system level the redistribution of joint load in the surrounding bone after implantation.[8,10,11,13,15,17]

Before determining the failure mechanism in the glenoid, it is first necessary to gain an understanding of the load transfer through the glenoid before and after reconstruction similar to hip and knee studies. We developed an FE model of a scapula with and without a virtually-implanted modern glenoid prosthesis design to determine how load transfer and stress distribution are affected by the introduction of a glenoid implant, by physiological alterations in the location and magnitude of the joint load on the glenoid, and by the presence of a metal-backing.

3.2 Materials and Methods

3.2.1 Study Design

The 3D geometry of an intact scapula was created based on CT scans of a left cadaver shoulder. A commercially available cemented and pegged polyethylene glenoid prosthesis was implanted simulating a TSA. Details are provided below but briefly, two load magnitudes were considered: normal and high. Loading locations were simulated at the center and at four eccentric positions on the glenoid surface. The load carried by the bone, cement, and implant, as well as the local stresses generated in the cement layer and glenoid, were determined and compared among the loading scenarios.

3.2.2 FE model

The left scapula of a cadaver (93 year old Caucasian female) with no apparent pathology was CT scanned at 1 mm intervals in the transverse plane. The 3D geometry of the scapula was developed from the scans using Mimics software (v 12.0, Materialise, Belgium). Two models were created: an intact scapula and a reconstructed scapula with a virtually-implanted glenoid prosthesis**.** In the latter model, only the face of the glenoid was reamed to match the flat-backed geometry of the back of the prosthesis. The prosthesis was virtually implanted to recreate the native version, which is neutral to the long axis of the scapular body according to recommendations by a surgeon. The prosthesis (Comprehensive®, Biomet, Warsaw, IN) was a three-pegged, asymmetric, all-polyethylene, cemented implant with a radius of curvature of 38.1 mm and was surrounded in the model by a uniform 1 mm cement layer (Fig. 3.1A). The pegs were modeled as cylindrical rods 10mm in length. In order to model a metal-backed prosthesis,

the cement material was given metallic properties as described below.

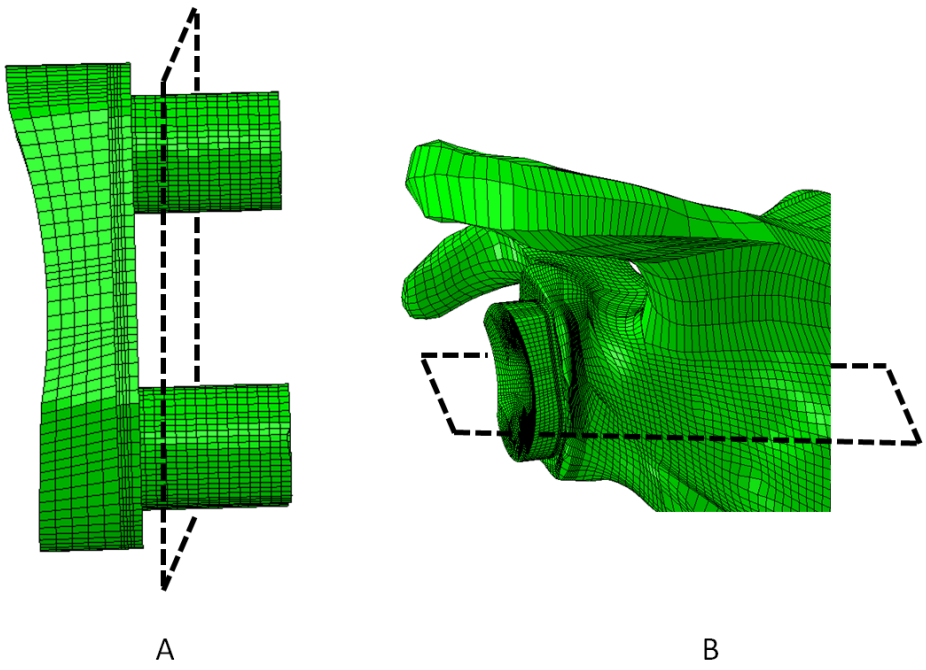

Figure 3.1 A) Posterior view of the glenoid implant and cement. The dashed plane shows a representative coronal layer used to analyze the load carried by the bone, cement, and implant. B) Posterior view of the scapula, showing the insertion of the glenoid implant. The dashed plane shows a representative transverse cross-section used in the analysis.

Eight-noded linear hexahedral elements were used to mesh the models using True Grid® software (XYZ Scientific Applications, v2.3.4, Inc, Livermore, CA). The scapula contained 30,945 elements; the glenoid implant and cement contained 33,509 elements. The number of elements was determined by a mesh convergence study that calculated the strain energy density within a region of interest in the glenoid (variance between consecutive models was <2%). The meshed model was then imported to ABAQUS (Simulia Corp, v6.9, Providence, RI) for analysis.

3.2.3 Material properties

To simplify the problem and save computational time, the scapular bone was modeled as isotropic and linearly elastic.[24] Because the densities of cancellous and cortical bone are heterogeneous in the glenoid and thus would affect load transfer,[13,27] the CT Hounsfield numbers for the bone pixels were related to the apparent densities by linear interpolation.[21] The densities were then correlated to elastic moduli using previously established relationships.[34,36] Given the cadaver's age, we increased the bone density uniformly by 20%, the approximate decrease in density from the age of 60 to 85.[35,38] A Poisson's ratio of 0.3 was used for bone.[7] The implant was made entirely of ultra high molecular weight polyethylene with a modulus and Poisson's ratio of 964 MPa and 0.34, respectively.[7] The cement was assigned a modulus of 2 GPa and a Poisson's ratio of 0.23.[7] To include a Ti alloy metal-backing, these values were replaced with those of Ti alloy (modulus and Poisson's ratio of 112 GPa and 0.33, respectively).[39]

3.2.4 Boundary and Loading Conditions

The scapula was held fixed at the medial border and at certain points on the acromion where it articulates with the acromioclavicular joint (Fig. 3.2A).[16,44] All interfaces (bone-cement, cement-implant, and bone-metal) were assumed to be fully bonded. A joint pressure ≈14 MPa was applied to the curved surface of the glenoid to simulate loading of a nonconforming reconstructed joint at 60° abduction, a motion commonly used in daily activities.[15] In addition, a second, higher pressure about three times higher was applied to the FE model to understand the effects of occasional high force activities, such as supporting oneself on crutches, standing up with support, or turning a blocked steering wheel.[2,4] The same loading conditions were applied to the intact model for consistency.

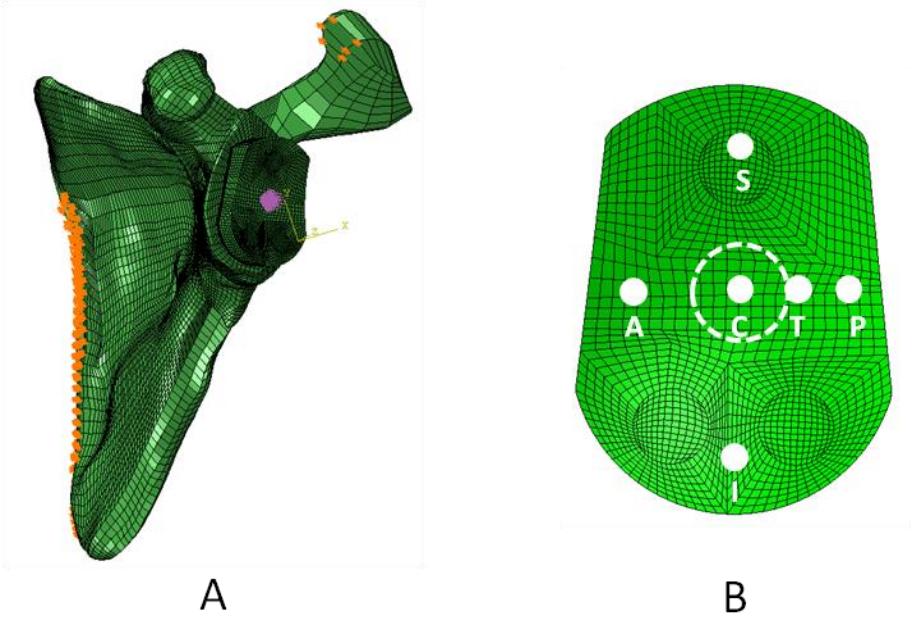

Figure 3.2 A) The applied boundary conditions on the reconstructed shoulder; the medial border is held fixed, and a center loading is applied to the implant surface indicated by the area in pink. B) Loading locations on the glenoid implant for center (C), transition (T), eccentric posterior (P), eccentric anterior (A), eccentric superior (S), and eccentric inferior (I). Filled circles indicate the approximate center of each loading area. Dashed circle represents the approximate surface area over which the load was applied. For all loading locations the load was applied over the same surface area.

We analyzed the effect of eccentric translation of the humeral head on the glenoid by applying the loading in the center of the glenoid, as well as in the anterior, superior, and inferior quadrants of the glenoid surface since observations from clinical and implant retrieval studies suggest significant in vivo eccentric translation (Fig. 3.2B).[19,29,32] Dominant loading in the posterior quadrant has been more commonly observed in cadaveric studies, in bi-planar in vivo fluoroscopic studies, and retrieved implants.[19,29,32,37] Therefore, we also applied a transition load between the center and eccentric posterior loading locations (Fig. 3.2B).

3.2.5 Data Analysis

Load transfer in the bone-implant system was determined by calculating the joint load carried by the bone, cement (or porous metal), and implant in nine evenly distributed lateral layers along the pegs moving progressively medially from the glenoid surface (Fig. 3.1A). The percent of the total load carried by the bone, cement, and implant was analyzed for each layer.

Maximum principal stresses were calculated in the cement layer as a means of assessing the potential for failure.[42] For bone, von Mises stresses were used as a failure criterion.[42] Both types of stress distributions were reported in a histogram showing the percent volume (of cement or bone) at different levels of stress for all loading conditions.[25] The average stress was found for each element, and then the elements were divided into groups with different stress levels. Spatial stress distributions were analyzed for transverse and coronal layers (Fig. 3.1).

3.3 Results

The majority of the applied joint load was carried by the bone even in the presence of the glenoid component. During centered loading, > 67% of the applied joint load was carried by the glenoid bone along the pegs (Fig. 3.3). The cement carried between 13 and 24% of the load depending on the position along the pegs, while the polyethylene pegs carried between 3 and 11% of the joint load. The joint load carried by the bone increased rapidly near the proximal end of the peg, coincident with the pegs approaching the cortical bone region. Even as the location of the applied load moved progressively posterior, the load carried by the bone remained above 60% (Fig. 3.4). In fact, the loading distributions among the bone, cement, and implant remained relatively consistent regardless of the location of the applied load (Figs. 3.3 and 3.4). Increasing

the bone mineral density by 20% to simulate a younger patient did not affect the load and stress distributions.

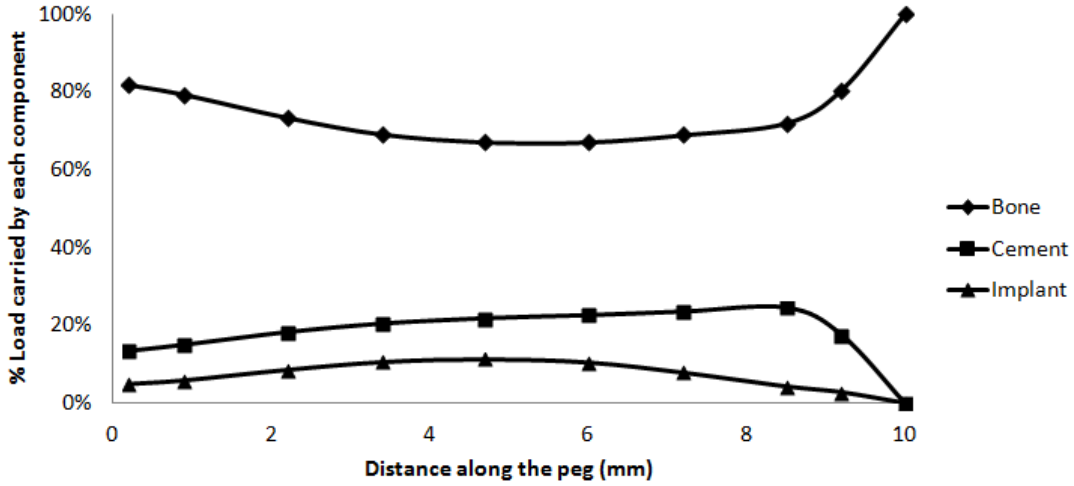

Figure 3.3 The percent of the joint load carried by the bone, cement, and implant during normal magnitude, center loading along the length of the peg. Similar trends were determined regardless of loading location. The cemented peg begins at 0mm and ends at 9mm. The data point at 10mm indicates the loading where no peg is present.

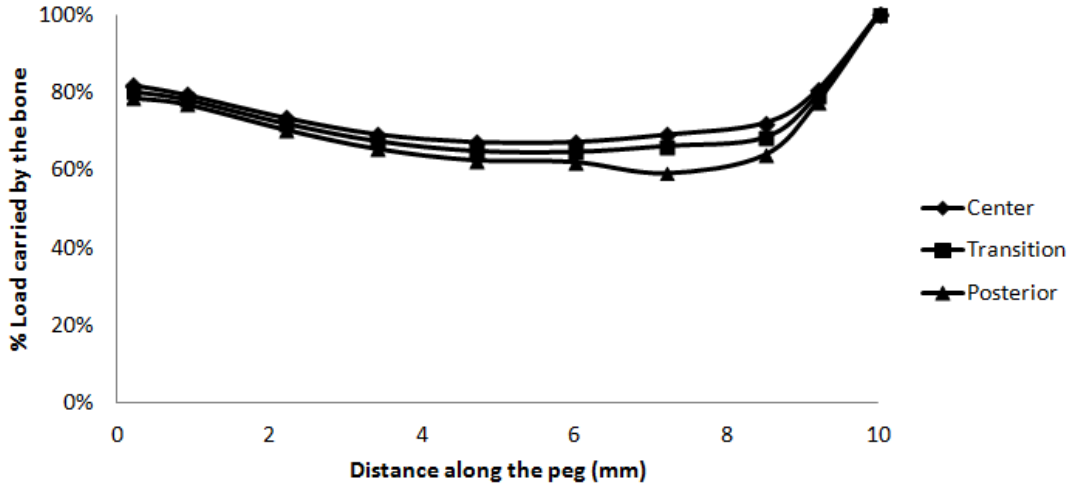

Figure 3.4 Percent of the joint load carried by the bone for center, transition, and posterior loading along the length of the cemented peg during normal magnitude load. The peg begins at 0mm and ends at 9mm. The data point at 10mm indicates the loading where no peg is present.

Load transfer patterns changed between the intact and reconstructed glenoids (Fig. 3.5). In the intact glenoid for both center and eccentric loading, the majority of stress was distributed in the cancellous bone (Fig. 3.5A and 3.5C). In the proximal region, the stresses were concentrated in the outer cortical layer of the scapular body. With the introduction of a cemented TSA implant, stresses were observed in the cortical bone of the scapular body only beyond the proximal end of all three pegs (Fig. 3.5B and 3.5D). Stresses in the cancellous bone underneath the glenoid component were lower than observed in the intact glenoid.

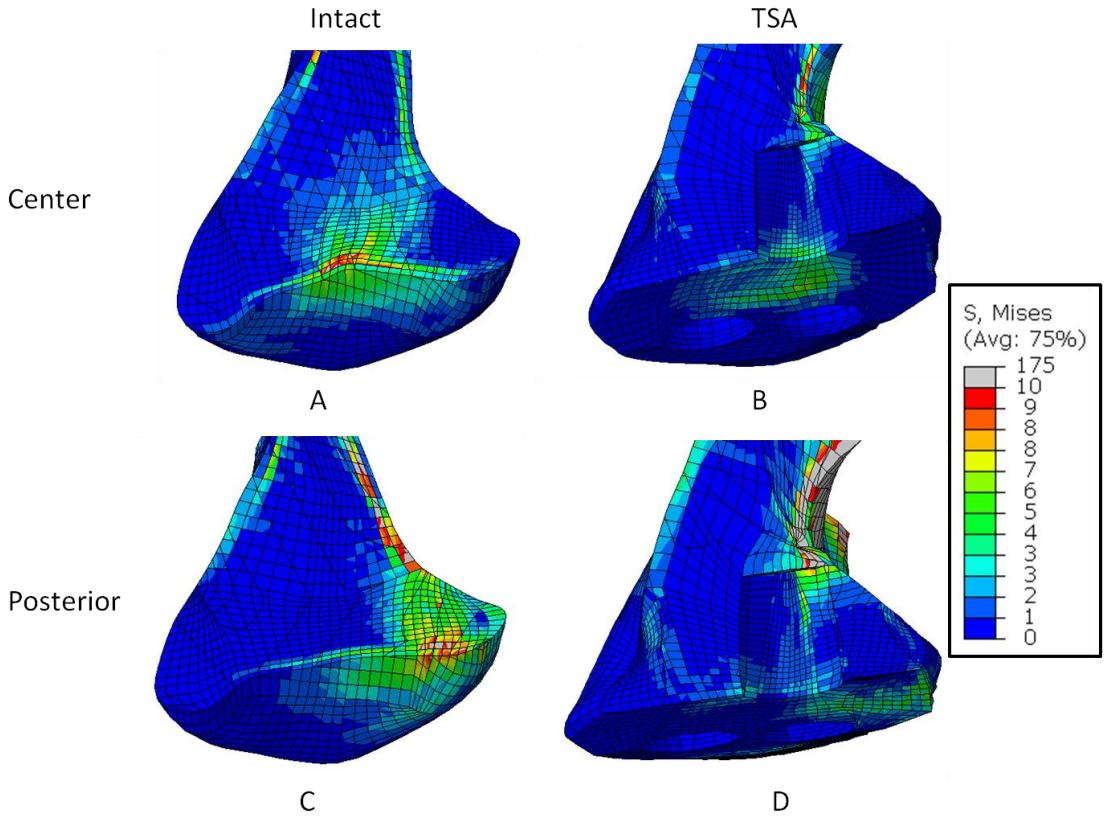

Figure 3.5 Superior views of transverse cross-sections of von Mises stress distributions in the glenoid for A) intact and B) reconstructed models during normal magnitude, center loading and C) intact and D) reconstructed models during normal magnitude, posterior eccentric loading. The areas in gray indicate stresses >10MPa.

Stresses in the cement layer increased when the loading changed from center to eccentric posterior loading (Fig. 3.6). This overall increase in stress was observed for the other eccentric loading conditions as well. Compressive stresses were present in the region where eccentric loading was applied, and tensile stresses on the opposite side (Fig. 3.7).

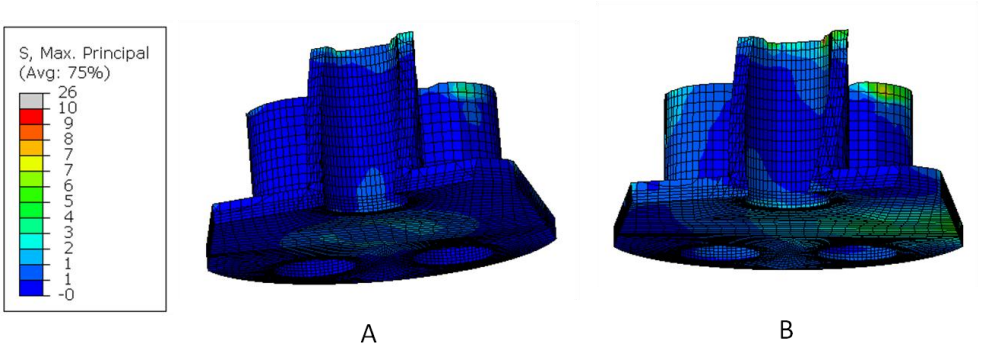

Figure 3.6 Superior views of maximum principal stress distributions in the cement layer during A) center and B) eccentric posterior loading for a normal magnitude load. The superior part of the superior peg is cut away to better visualize the stresses inside the cement layer.

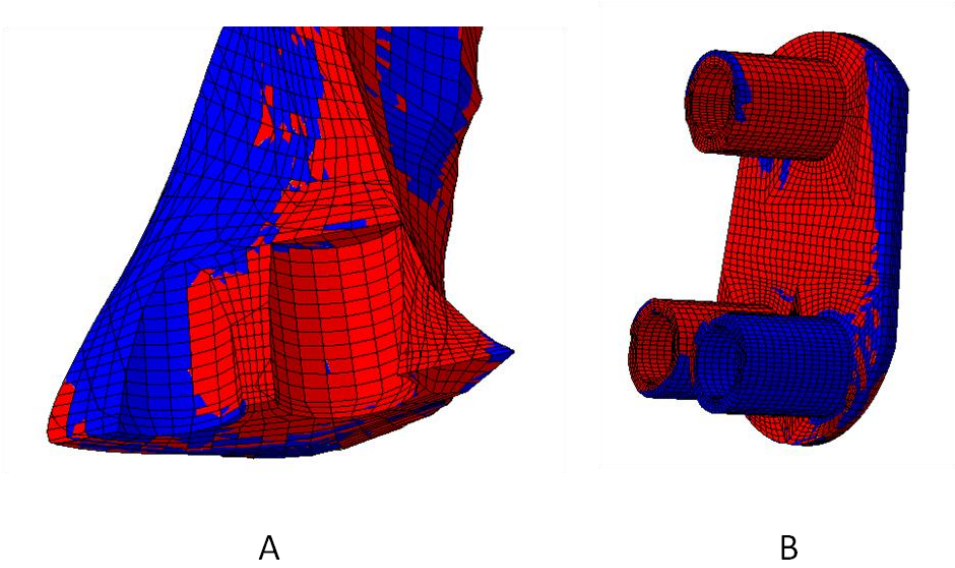

Figure 3.7 Stress distribution in the medial-lateral direction: A) Superior view of a transverse cross-section of the glenoid; B) Anterior view of the backside of the cement layer. Areas in red represent compressive stresses, and areas in blue represent tensile stresses.

When the implant was metal-backed, a greater percent of the applied joint load was carried by the implant (including the metal-backing) than in the case of an all-polyethylene cemented implant (Fig. 3.8). The joint load carried by the bone was as low as 42%, with the metal-backing carrying as much as 57%. The load carried by the bone in the metal-backed model was reduced by 25 to 40% below that in the cemented model during center loading. Furthermore, the metal-backed implant lowered the stresses in the glenoid bone (Figs. 3.9A and 3.9B) with concomitant higher stresses in the metal-backing (Figs. 3.9C and 3.9D) compared to a cemented TSA.

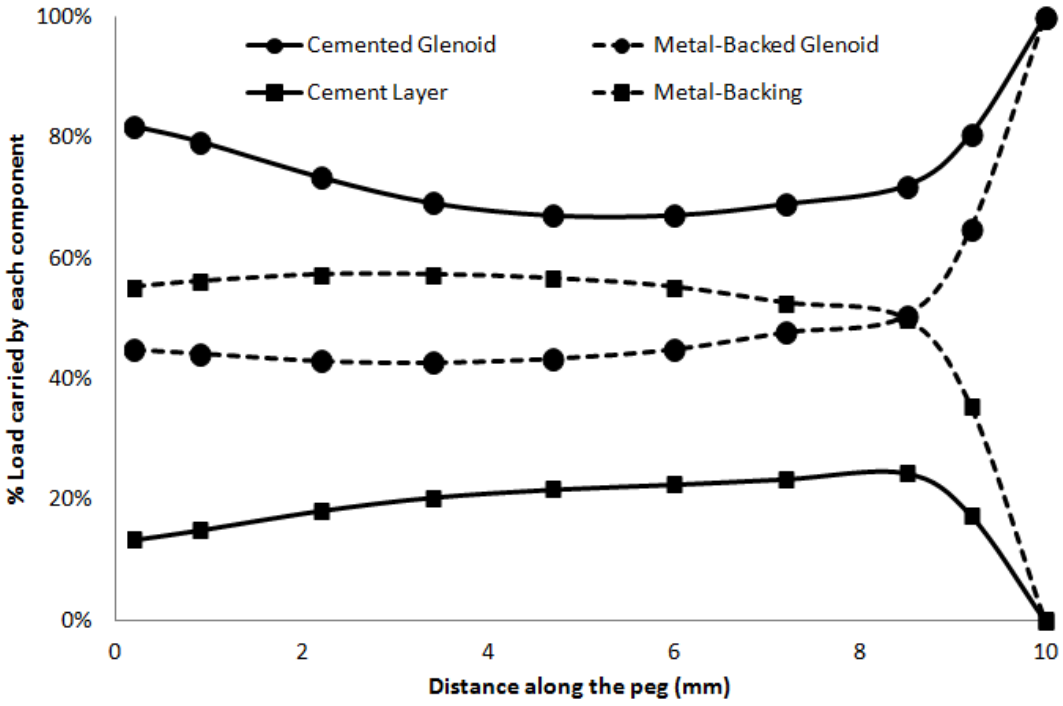

Figure 3.8 Joint load carried by the bone in a cemented polyethylene glenoid implant and a metal-backed polyethylene glenoid implant during normal magnitude, center loading. The data point at 0 mm indicates the lateral end of the peg and 10mm indicates the loading where no peg is present.

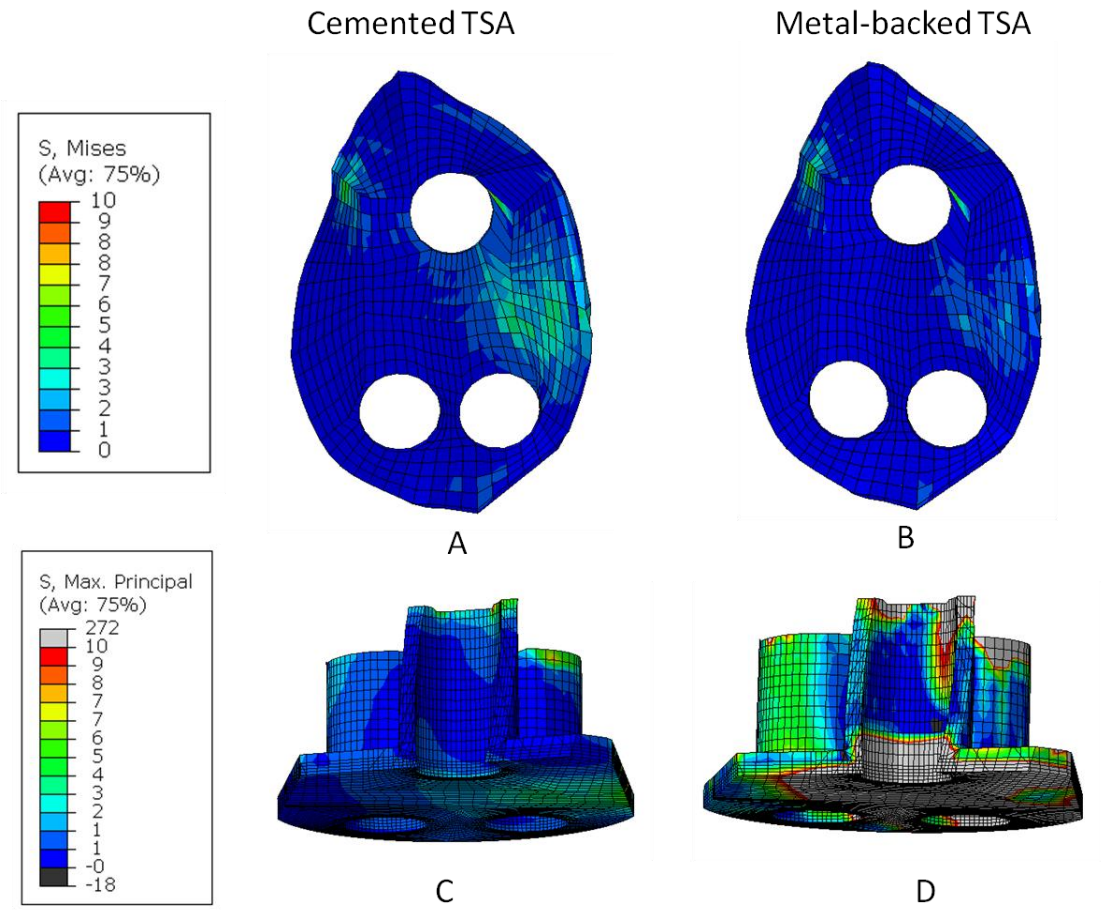

Figure 3.9 Lateral views of representative coronal cuts of von Mises stress distributions in the glenoid bone in A) cemented and B) metal-backed TSA models during normal magnitude, eccentric posterior loading. Superior views of maximum principal stress distributions in the C) cement layer and D) metal-backing during posterior loading. The superior part of the superior peg is cut away to better visualize the stresses inside the cement layer. The areas in gray indicate stresses >10MPa.

Similar bone stress distributions were observed in the glenoid between the intact and reconstructed models for normal and high magnitude loads (Fig. 3.10). During posterior loading for a normal magnitude load, the majority of stresses in a representative bone layer ranged between 0 and 4 MPa. However, with a high magnitude load, about 15% of the bone volume was stressed between 4 and 10 MPa, and the overall stress in the bone increased with load magnitude regardless of loading location and across all the bone layers (Fig. 3.10).

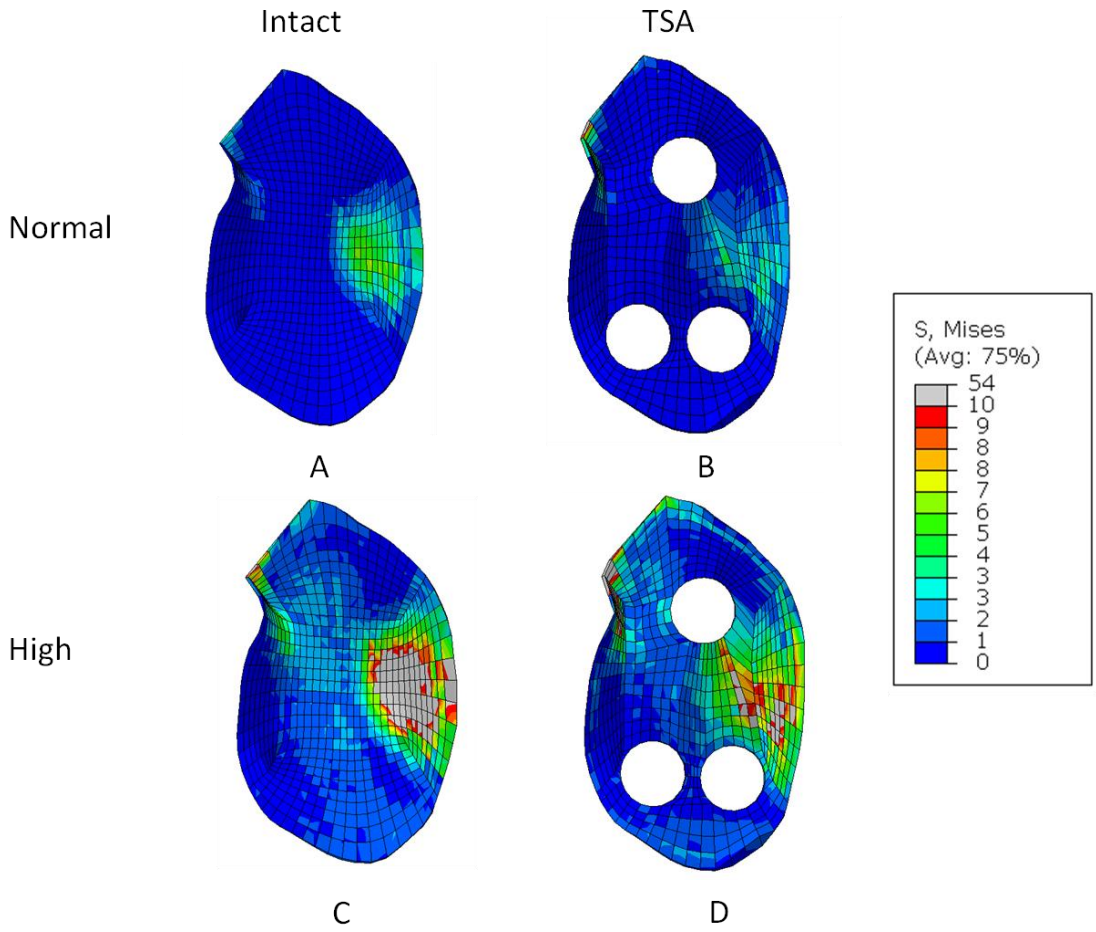

Figure 3.10 von Mises stress distributions in bone for the intact and reconstructed scapulas during eccentric posterior loading under normal and high magnitude loads. (A) Intact shoulder with normal-magnitude loading, (B) TSA with normal-magnitude loading, (C) Intact shoulder with high-magnitude loading, and (D) TSA with high-magnitude loading. One layer is shown for simplicity; however, similar trends occurred for other layers along the peg. Similar results were found during center loading as well. The areas in gray indicate stresses >10MPa.

Similarly, in the cement layer, stresses increased as the load magnitude increased (Fig. 3.11). For a normal load, most of the cement (~94%) was stressed between 0 and 4 MPa during eccentric posterior loading. For the high magnitude load, 21% of the cement volume was stressed >4 MPa. Similar trends were observed with the other loading locations. Spatial stress distributions in the cement demonstrated the increase in stress during high magnitude loading (Fig. 3.11).

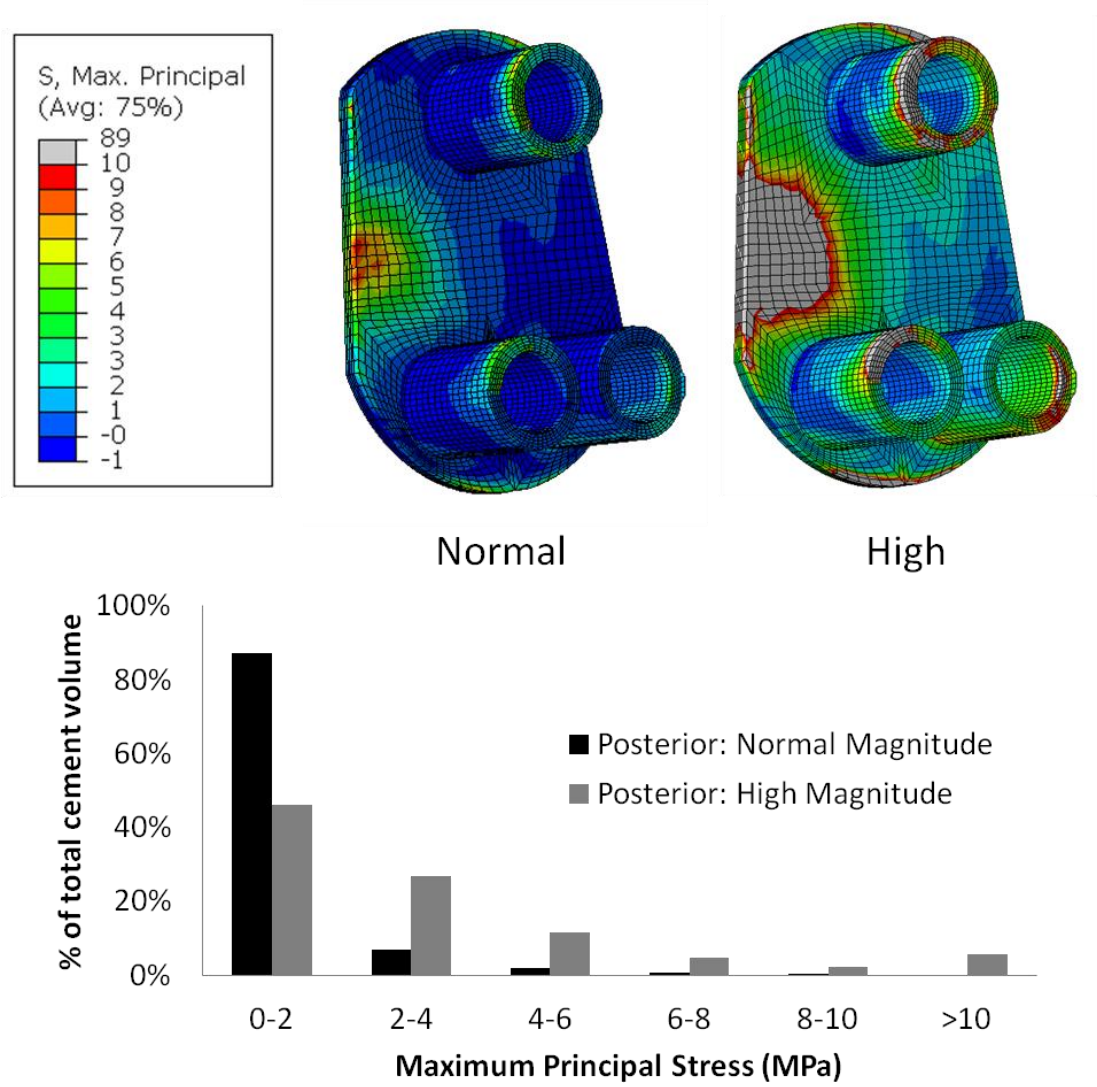

Figure 3.11 Spatial stress distributions and a histogram of maximum principal stresses in the cement layer during eccentric posterior loading for normal and high magnitude load. Similar trends were observed for center loading.

3.4 Discussion

Our results can be used to interpret the fundamentals of joint load transfer in the intact glenoid and in the reconstructed glenoid after TSA. Our first research question dealt with the effects on load transfer and stress distribution in the glenoid after the introduction of a glenoid implant. Introduction of the cemented TSA implant significantly altered the load transfer pattern

in the glenoid. In the intact glenoid, the joint load was initially transferred to the underlying cancellous bone, and then gradually to the cortical bone lining the scapular body. With the insertion of the glenoid implant, the load was redistributed so that the cement and implant carried a considerable amount of the load. Only beyond the tip of the pegs did the cortical bone carry a large portion of the load (Fig. 3.3 and 3.5). Load carried by the bone along the pegs can be divided into three regions: in the lateral region, the load decreased; in the middle, the load remained the same; and proximally, the load rapidly increased to 100%. The decrease in load carried by the bone in the lateral region suggests that the load in the bone was gradually transferred to the cement and implant. In the middle region, the cement and implant steadily carried a significant portion of the load. Towards the proximal end of the pegs, the load shared by the cement and implant was gradually transferred back to the bone, and more specifically to the cortical bone. Since the load is more likely to be carried by stiff bone regions at the proximal end of the pegs, the load is transferred to the stiffer cortical bone rather than the less stiff cancellous bone. This finding was supported by the gradually increased stresses observed in the cortical bone moving proximally.

The change in loading pattern observed in the reconstructed glenoid is similar to what has been previously observed in stemmed total hip femoral components and total knee tibial components. In the case of the femoral component, the stem is well-fixed distally and also stiff enough to carry the majority of the applied joint load.[11] For the tibial component, the stem is long enough to engage and is rigidly fixed to the distal cortex.[30] In both cases, stress shielding of the cancellous bone near the joint is the main cause of loosening. The introduction of the stem causes the joint load to bypass cancellous bone, which decreases stress in the bone resulting in bone resorption. We observed a similar pattern in the three-pegged glenoid component where

load in the cancellous bone was bypassed to distal cortical bone with introduction of the glenoid implant. Thus, even with an all-polyethylene implant, the pegs surrounded by cement is stiffer than the surrounding bone, and as a result carries the load normally carried by cancellous bone in the intact glenoid. Shorter pegs that would end in the middle of the cancellous bone region would allow load to be transferred to the cancellous bone sooner and possibly decrease the likelihood for stress shielding by increasing stress in this area.

Our second research question was concerned with how changes in the location and magnitude of the applied joint load affected load transfer and the local stress distributions in the reconstructed glenoid. The observed compressive stress on the posterior side and tensile stress on the anterior side of the glenoid confirms the "rocking horse" phenomenon, with higher stresses in the cement layer, suggesting that cement failure is likely with eccentric loading. However, whether the interface fails or the cement fails is open to interpretation, but either one could lead to glenoid loosening.

When a high magnitude joint load was applied, maximum principal stresses in the cement increased significantly, suggesting increased risk of cement failure. The fatigue strength of cement is 10 MPa at 1 million cycles[31] and 3.3 MPa at 10 million cycles.[24] Our results showed that with high eccentric posterior loading, 21% of the cement volume was stressed beyond 4 MPa, and about 4.5% of the cement volume was stressed above 10 MPa, suggesting that cement failure is indeed a likely scenario.

Our third research question dealt with the effects of a metal-backed glenoid implant after a TSA. Changing the cement layer to a metal-backing had no effect on the load-sharing pattern in the bone-implant system; however, the metal-backing carried a higher percent of the load relative to the cement layer due to the high stiffness of the metal-backing. The load was carried

to the stiffer cortical bone at the proximal end of the pegs. This situation is comparable to use of the metal-backed tibial component in total knee replacement where stresses are directed away from proximal, less stiff cancellous bone to distal, stiffer cortical bone.[3] The lower stresses observed in the cancellous bone agree with other numerical studies that also suggested stress shielding caused by the high stiffness of the metal backing,[15,39] and support clinical observations of osteolysis and high rates of loosening in metal-backed glenoid implants.[40,45]

Since our study was based on one bone, our results should be interpreted in terms of the general effects of introduction of an implant, of physiological alterations in the location and magnitude of the joint load on the glenoid, and of the presence of a metal-backing. Anatomical variables vary from individual to individual, however the aim of this study was not to predict specific stresses in a particular person, and therefore comparison of these stresses must be interpreted accordingly. The use of a healthy joint is a limitation since bony anatomy is affected by osteoarthritis, however the use of healthy joints is a common method used in similar computational modeling studies in the literature.[26,42,43] The bone was modeled as linear elastic, a reasonable assumption even during high loading since less than 5% of the bone volume was stressed beyond the yield strength. Also, we assumed fully bonded interfaces representative of a well-functioning TSA. If this assumption were relaxed, we would expect higher stresses at the interfaces, especially during eccentric loading. Similarly, we assumed an even 1mm layer of cement was distributed around the implant. Although we followed surgical recommendations, in reality this may not be the case, and cause higher stress at the interfaces. Finally, we wanted to understand the effect of a stiffer fixation layer and changed the material properties of the cement layer to those of Ti alloy. Although replacing the cement layer with a metal layer is not an accurate representation of a commercially available metal-backed implant, we would expect the

current results to be a conservative estimate of how metal-backed implants affect load transfer in the glenoid after reconstruction.

3.5 Conclusion

In conclusion, using an FE model to examine load transfer in the glenoid before and after a TSA, we provided a basic understanding of the load sharing phenomenon after a TSA that could explain glenoid loosening failure. Our results suggest that with reconstruction of the glenoid with a contemporary implant, the load transfer pattern changes, with eccentric and high magnitude loads increasing stresses in the cement. The use of a metal-backed implant reduces the load carried by the bone, which may be detrimental to long term TSA survival. We hope to apply the model in further studies to explore comparative changes in load transfer and stresses under differing clinical, surgical, and design conditions.

REFERENCES

1. Andriacchi TP, Stanwyck TS, Galante JO. Knee biomechanics and total knee replacement. J Arthroplasty. 1986;1(3):211–9.

2. Anglin C, Wyss UP, Pichora DR. Glenohumeral contact forces. Proc Inst of Mech Eng. H. 2000;214(6):637–44.

3. Bartel DL, Burstein AH, Santavicca EA, Insall JN. Performance of the tibial component in total knee replacement. J Bone Joint Surg Am. 1982;64(7):1026–33.

4. Bergmann G, Graichen F, Bender A, Kääb M, Rohlmann A, Westerhoff P. In vivo glenohumeral contact forces--measurements in the first patient 7 months postoperatively. J Biomech. 2007;40(10):2139–49. doi:10.1016/j.jbiomech.2006.10.037

5. Bohsali KI, Wirth MA, Rockwood CA. Complications of total shoulder arthroplasty. J Bone Joint Surg Am. 2006;88(10):2279–92. doi:10.2106/JBJS.F.00125

6. Boileau P, Avidor C, Krishnan SG, Walch G, Kempf J-F, Molé D. Cemented polyethylene versus uncemented metal-backed glenoid components in total shoulder arthroplasty: a prospective, double-blind, randomized study. J Shoulder Elbow Surg. 2002;11(4):351–9. doi:10.1067/mse.2002.125807

7. Couteau B, Mansat P, Estivalèzes E, Darmana R, Mansat M, Egan J. Finite element analysis of the mechanical behavior of a scapula implanted with a glenoid prosthesis. Clin Biomech. 2001;16(7):566–75.

8. Ducheyne P, Kagan A, Lacey J. Failure of total knee arthroplasty due to loosening and deformation of the tibial component. J Bone Joint Surg Am. 1978;60(3):384–391.

9. Edwards TB, Labriola JE, Stanley RJ, O'Connor DP, Elkousy HA, Gartsman GM. Radiographic comparison of pegged and keeled glenoid components using modern cementing techniques: a prospective randomized study. J Shoulder Elbow Surg. 2010;19(2):251–7. doi:10.1016/j.jse.2009.10.013

10. Engh CA, Bobyn JD, Glassman AH. Porous-Coated Hip Replacement The Factors Governing Bone Ingrowth, Stress Shielding, and Clinical Results. J Bone Joint Surg Br. 1987;69(1):45–55.

11. Engh CA, McGovern T, F, Bobyn JD, Harris WH. A quantitative evaluation of periprosthetic bone-remodeling after cementless total hip arthroplasty. J Bone Joint Surg Am. 1992;74(7):1009–1020.

12. Franklin JL, Barrett WP, Jackins SE, Matsen FA. Glenoid loosening in total shoulder arthroplasty. Association with rotator cuff deficiency. J Arthroplasty. 1988;3(1):39–46.

13. Frich H, Jensen NC, Odgaard A, Pedersen CM, Sojbjerg JO, Dalstra M. Bone strength of the glenoid and material properties. J Shoulder Elbow Surg. 1997;6(2):97–1104.

14. Gross S, Abel EW. A finite element analysis of hollow stemmed hip prostheses as a means of reducing stress shielding of the femur. J Biomech. 2001;34(8):995–1003.

15. Gupta S, van der Helm FCT, van Keulen F. The possibilities of uncemented glenoid component--a finite element study. Clin Biomech. 2004;19(3):292–302. doi:10.1016/j.clinbiomech.2003.12.002

16. Gupta S, van der Helm FCT. Load transfer across the scapula during humeral abduction. J Biomech. 2004;37(7):1001–9. doi:10.1016/j.jbiomech.2003.11.025

17. Harris WH, Sledge CB. Total Hip and Total Knee Replacement. N Engl J Med. 1990;323(11):725–731.

18. Hayes WC, Swe LW, Schurman DJ. Axisymmetric finite element analysis of the lateral tibial plateau. J Biomech. 1978;11(1):21–33.

19. Hertel R, Ballmer FT. Observations on retrieved glenoid components. J Arthroplasty. 2003;18(3):361–6. doi:10.1054/arth.2003.50048

20. Huiskies R, Weinans H, Grootenboer HJ, Dalstra M, Fudala B, Slooff TJ. Adaptive Bone-Remodeling Theory Applied to Prosthetic-Design Analysis. J Biomech. 1987;20(11):1135–1150.

21. Hvid I, Bentzen SM, Linde F, Mosekilde L, Pongsoipetch B. X-ray quantitative computed tomography: the relations to physical properties of proximal tibial trabecular bone specimens. J Biomech. 1989;22(8-9):837–44.

22. Junaid S, Gupta S, Sanghavi S, Anglin C, Roger E, Amis A, et al. Failure mechanism of the all-polyethylene glenoid implant. J Biomech. 2010;43(4):714–9. doi:10.1016/j.jbiomech.2009.10.019

23. Keaveny TM, Bartel DL. Effects of porous coating and collar support on early load transfer for a cementless hip prosthesis. J Biomech. 1993;26(10):1205–16.

24. Lacroix D, Murphy LA, Prendergast PJ. Three-dimensional finite element analysis of glenoid replacement prostheses: a comparison of keeled and pegged anchorage systems. J Biomech Eng. 2000;122(4):430–6.

25. Lennon A, Prendergast PJ. Evaluation of cement stresses in finite element analyses of cemented orthopaedic implants. J Biomech Eng. 2001;123(6):623–628.

26. Long JP, Bartel DL. Surgical variables affect the mechanics of a hip resurfacing system. Clin Orthop Relat Res. 2006;453:115–22. doi:10.1097/01.blo.0000238873.09390.6f

27. Mansat P, Barea C, Hobatho M-C, Darmana R, Mansat M. Anatomic variation the glenoid of the mechanical properties of the glenoid. J Shoulder Elbow Surg. 1998;7(2):109–115.

28. Mansat P, Briot J, Mansat M, Swider P. Evaluation of the glenoid implant survival using a biomechanical finite element analysis: influence of the implant design, bone properties, and loading location. J Shoulder Elbow Surg. 2007;16(3):S79–S83. doi:10.1016/j.jse.2005.11.010

29. Massimini DF, Li G, Warner JP. Glenohumeral contact kinematics in patients after total shoulder arthroplasty. J Bone Joint Surg Am. 2010;92(4):916–26. doi:10.2106/JBJS.H.01610

30. Murase K, Crowninshield RD, Pedersen DR, Chang TS. An analysis of tibial component design in total knee arthroplasty. J Biomech. 1983;16(1):13–22.

31. Murphy BP, Prendergast PJ. On the magnitude and variability of the fatigue strength of acrylic bone cement. Int J Fat. 2000;22(10):855–864.

32. Nho SJ, Nam D, Ala OL, Craig E V, Warren RF, Wright TM. Observations on retrieved glenoid components from total shoulder arthroplasty. J Shoulder Elbow Surg. 2009;18(3):371–378. doi:10.1016/j.jse.2008.12.006

33. Nuttall D, Haines JF, Trail II. A study of the micromovement of pegged and keeled glenoid components compared using radiostereometric analysis. J Shoulder Elbow Surg. 2004;16(3):S65–70. doi:10.1016/j.jse.2006.01.015

34. Rice JC, Cowin SC, Bowman JA. On the dependence of the elasticity and strength of cancellous bone on apparent density. J Biomech. 1988;21(2):155–68.

35. Russo C, Lauretani F, Bandinelli S, Bartali B, Di lorio A, Volpato S, et al. Aging bone in men and women: beyond changes in bone mineral density. Osteoporos Int. 2003;14(7):531–538. doi:10.1007/s00198-002-1322-y

36. Schaffler MB, Burr DB. Stiffness of compact bone: effects of porosity and density. J Biomech. 1988;21(1):13–6.

37. Soslowsky LJ, Flatow EL, Bigliani LU, Pawluk RJ, Ateshian GA, Mow VC. Quantitation of in situ contact areas at the glenohumeral joint: a biomechanical study. J Orthop Res. 1992;10(4):524–34. doi:10.1002/jor.1100100407

38. Steiger P, Cummings SR, Black DM, Spencer NE, Genant HK. Age-related decrements in bone mineral density in women over 65. J Bone Miner Res. 1992;7(6):625–32. doi:10.1002/jbmr.5650070606

39. Stone KD, Grabowski JJ, Cofield RH, Morrey BF, An KN. Stress analyses arthroplasty of glenoid components in total shoulder. J Shoulder Elbow Surg. 1999;8(2):151–8.

40. Tammachote N, Sperling JW, Vathana T, Cofield RH, Harmsen WS, Schleck CD. Long-term results of cemented metal-backed glenoid components for osteoarthritis of the shoulder. J Bone Joint Surg Am. 2009;91(1):160–6. doi:10.2106/JBJS.F.01613

41. Taunton MJ, McIntosh AL, Sperling JW, Cofield RH. Total shoulder arthroplasty with a metal-backed, bone-ingrowth glenoid component. Medium to long-term results. J Bone Joint Surg Am. 2008;90(10):2180–8. doi:10.2106/JBJS.G.00966

42. Terrier A, Büchler P, Farron A. Bone-cement interface of the glenoid component: stress analysis for varying cement thickness. Clin Biomech. 2005;20(7):710–7. doi:10.1016/j.clinbiomech.2005.03.010

43. Terrier A, Büchler P, Farron A. Influence of glenohumeral conformity on glenoid stresses after total shoulder arthroplasty. J Shoulder Elbow Surg. 2006;15(4):515–20. doi:10.1016/j.jse.2005.09.021

44. Veeger HEJ, van der Helm FCT. Shoulder function: the perfect compromise between mobility and stability. J Biomech. 2007;40(10):2119–29. doi:10.1016/j.jbiomech.2006.10.016

45. Wirth MA, Rockwood CA. Current Concepts Review - Complications of Total Current Concepts Review Complications of Total Shoulder-Replacement Arthroplasty. J Bone Joint Surg Am. 1996;78(4):603–16.

46. Yian EH, Werner CML, Nyffeler RW, Pfirrmann CW, Ramappa A, Sukthankar A, et al. Radiographic and computed tomography analysis of cemented pegged polyethylene glenoid components in total shoulder replacement. J Bone Joint Surg Am. 2005;87(9):1928–36. doi:10.2106/JBJS.D.02675

Chapter 4

The Effects of Osteoarthritis on Load Transfer After Cemented Total Shoulder Arthroplasty[3]

4.1 Introduction

Total shoulder arthroplasty (TSA) is commonly performed to treat glenohumeral osteoarthritis (OA); however, the complication rate of this surgery has been reported as high as 14.7%.[1] The most common complication is glenoid component loosening. Although implant designs have been created in attempts to reduce implant failure, the rate of radiolucencies is still as high as 36-83%.[27,38] Previous experimental and computational studies proposed conflicting failure mechanisms, suggesting that failure occurs in the bone, cement, or interface.[18,19,22,34,38]

Load transfer patterns and local stress distributions in the bone-implant system are the common focus of most mechanical analyses of TSA.[3,28,34] In a previous study, we showed that high magnitude and eccentric loading increased tensile stresses in the cement layer and surrounding glenoid bone.[28] We also showed that the compressive joint load bypassed the

[3] Patel R, Gulotta L, Wright T, Gao Y. The Effects of Osteoarthritis on Load Transfer after a Cemented Total Shoulder Arthroplasty. Journal of Shoulder and Elbow Surgery. 2014 (Under Review)

cancellous bone region and was transferred directly to the scapular cortical shell when the ends of the implant pegs were in close proximity to the scapular cortical bone of a healthy joint.[28] We do not know, however, if the same load transfer pattern would occur when the ends of the pegs were further away from the cortical bone. We also do not know if the same load transfer pattern would be observed in an osteoarthritic (OA) shoulder.

OA is associated with increased bony density and retroversion of the glenoid that could affect load transfer in the bone-implant system.[2,4,6,17,26,31,33] However, most finite element (FE) studies have focused on understanding the local stresses generated in the reconstructed healthy specimen. Mansat et al modeled eccentric loading in the OA shoulder with keeled and pegged components, but did not comment on the effect of bone density or retroversion.[22] Furthermore, the effect of retroversion has only been modeled in healthy specimens.[6,35] Farron et al determined that with retroversion, the contact location on the glenoid moved posteriorly and stresses increased in the cement layer and in glenoid bone.[6] However, the scapula was a healthy specimen. Terrier et al also found increased posterior contact on the glenoid causing an increase in cement and bone-cement interface stresses with increased retroversion, but again a healthy specimen was modeled.[35]

Increased retroversion (typically > 10°) can lead to eccentric contact on the glenoid.[6,26] The "rocking horse" phenomenon induced by eccentric loading is commonly attributed to glenoid loosening.[7,37] Current surgical procedures aim to correct excessive retroversion using methods such as posterior bone-grafting, or more commonly by reaming the anterior part of the glenoid to correct version.[6,14,26] Unfortunately significant eccentric posterior contact remains in TSA patients with anteriorly reamed glenoids.[23]

We sought to establish the effects of OA- induced changes in bone density and retroversion angle on load transfer and stress distribution in the bone-implant system of the scapula. Two specific questions were addressed: (1) how does implant peg proximity to cortical bone affect load transfer in OA as compared to healthy glenoids; and (2) how are local stress distributions and load transfer affected among healthy, retroverted OA, and corrected OA glenoids under central and eccentric joint loads? To answer these questions, we developed FE models of a healthy and OA reconstructed scapula implanted with a contemporary glenoid component. Stress distributions in the bone-implant system, and load carried by cement, implant and bone were determined and compared among the models.

4.2 Materials and Methods

4.2.1 Study Design

Models of two scapulas, one healthy and the other osteoarthritic, were created from CT scans of two left cadaver scapulas. The geometry and properties of a commercially available cemented and pegged polyethylene glenoid component were incorporated in both models. For the OA scapula, two models were created, one with retroversion and one with retroversion corrected. Normal loads were applied at the center or posteriorly on the glenoid surface. The load carried by the bone, cement, and implant and the local stresses generated in the cement layer and glenoid, were determined and compared among the models and the loading scenarios.

4.2.2 FE model

The left scapulas of a healthy (93 yr-old female) and an osteoarthritic (61 yr-old female)

shoulder were CT scanned at <1 mm intervals in the transverse plane. The 3D scapular geometry was developed from the scans using Mimics software (v 12.0, Materialise, Belgium). Three models were created: a reconstructed healthy scapula, a retroverted OA scapula with 18° of retroversion, and a corrected OA scapula with 6° of retroversion. The reconstructed scapula included a virtually-implanted glenoid prosthesis (Comprehensive®, Biomet, Warsaw, IN). The prosthesis was a three-pegged, asymmetric, all-polyethylene, cemented implant with a radius of curvature of 38.1 mm and was surrounded in the model by a uniform 1 mm cement layer (Fig. 4.1A). The face of the glenoid was reamed to match the flat-backed geometry of the prosthesis. For the healthy scapula, the prosthesis was virtually implanted to recreate native version, which is neutral to the long axis of the scapular body. The pegs were modeled as cylindrical rods 10mm in length. To investigate peg proximity to the cortical bone in the scapula, the peg lengths were lengthened or shortened by ~2.5mm. The implant pegs were defined as touching the cortex if they were either at or near the cortical bone or not touching if they were away from cortical bone and only in the cancellous bone region of the glenoid.

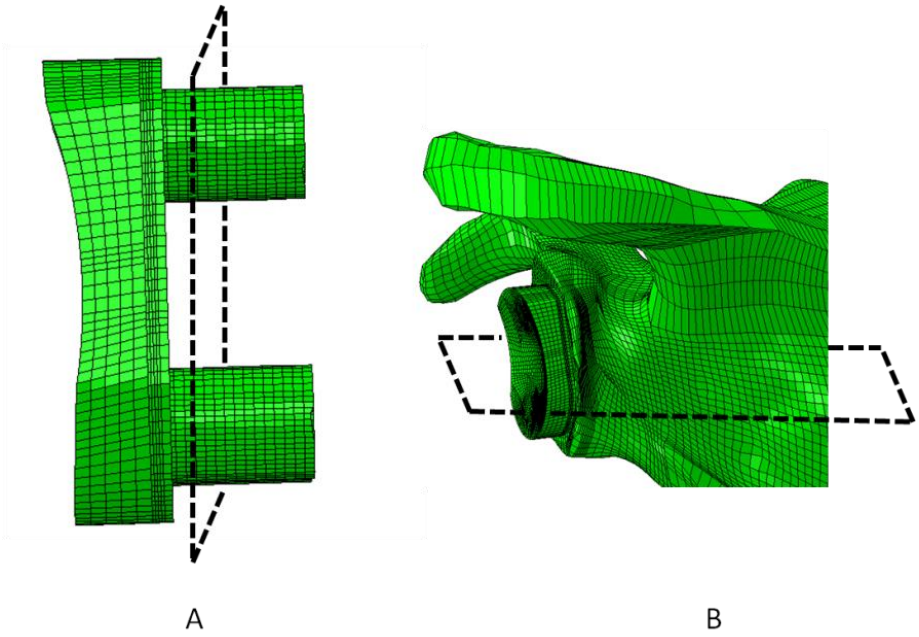

Figure 4.1: A) Posterior view of the glenoid implant and cement. The dashed plane shows a representative coronal layer used to analyze the load carried by the bone, cement, and implant. B) Posterior view of the scapula, showing the insertion of the glenoid implant. The dashed plane shows a representative transverse cross-section used in the analysis.

Eight-noded linear hexahedral elements were used to mesh the models using True Grid® software (XYZ Scientific Applications Inc, v2.3.4, Livermore, CA). The healthy scapula contained 30,945 elements; the glenoid implant and cement contained 33,509 elements. The OA scapula contained 37,434 elements. The number of elements was determined by a mesh convergence study that calculated the strain energy density within a region of interest in the glenoid (variance between consecutive models was <2%). The meshed model was then imported to ABAQUS (Simulia Corp, v6.9, Providence, RI) for analysis.

4.2.3 Material properties

To simplify the problem and save computational time, the scapular bone was modeled as isotropic and linearly elastic.[19] Because the densities of cancellous and cortical bone are

heterogeneous in the glenoid and thus would affect load transfer,[8,21] the CT Hounsfield numbers for the bone pixels were related to the apparent densities by linear interpolation.[16] The densities were then correlated to elastic moduli using previously established relationships.[29,30] A Poisson's ratio of 0.3 was used for bone.[3] Only one OA glenoid was modeled; however, three glenoids were analyzed confirming that overall stiffness increased with OA as is observed in the literature[4,5,24]. The implant was made entirely of ultra high molecular weight polyethylene with a modulus and Poisson's ratio of 964 MPa and 0.34, respectively.[3] The cement was assigned a modulus of 2 GPa and a Poisson's ratio of 0.23.[3]

4.2.4 Boundary and Loading Conditions

The scapula was held fixed at the medial border and at points on the acromion where it articulates with the acromioclavicular joint (Fig. 4.2A).[11,36] All interfaces (bone-cement and cement-implant) were assumed to be fully bonded. A joint pressure ≈14 MPa was applied to the curved surface of the glenoid to simulate loading of a nonconforming reconstructed joint at 60° abduction, a joint position commonly encountered during daily activities.[10] The same loading condition was applied to the intact models for consistency.

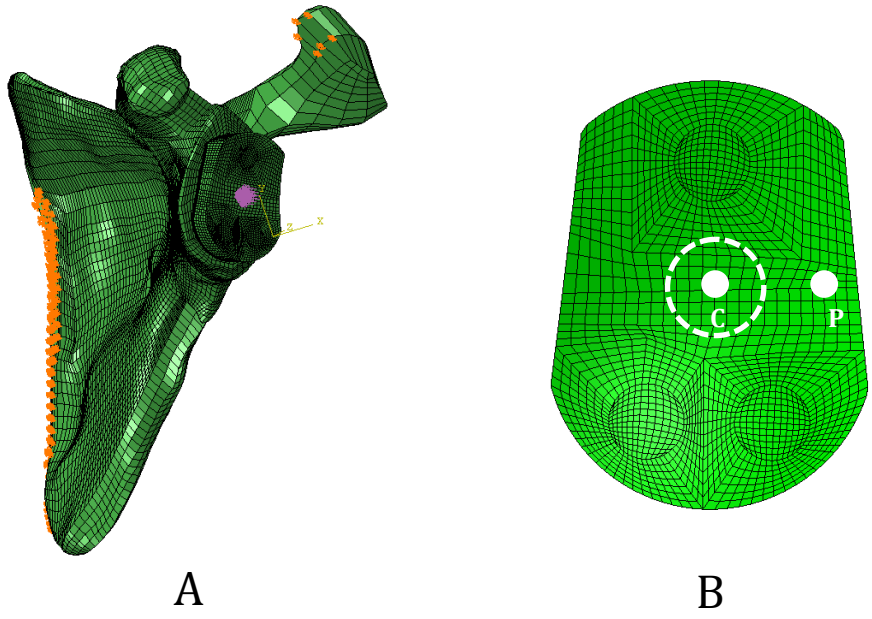

Figure 4.2: A) The applied boundary conditions on the reconstructed shoulder; the medial border is held fixed, and a center loading is applied to the implant surface indicated by the area in pink. B) Loading locations on the glenoid implant for center (C), and eccentric posterior (P). Filled circles indicate the approximate center of each loading area. Dashed circle represents the approximate surface area over which the load was applied. For all loading locations the load was applied over the same surface area.

We analyzed the effect of eccentric translation of the humeral head on the glenoid by applying the loading both in the center of the glenoid and in the posterior quadrant of the glenoid surface, since clinical and implant retrieval observations and cadaveric biomechanical studies suggest significant in vivo eccentric translation (Fig. 4.2B).[13,23,25,32]

4.2.5 Data Analysis

Load transfer in the bone-implant system was determined by calculating the percent of the total joint load carried by the bone, cement, and implant in evenly distributed lateral layers along the pegs moving progressively medially from the glenoid surface (Fig. 4.1A).

Maximum principal stresses were calculated in the cement layer as a means of assessing the potential for failure.[34] Stress distributions were reported in a histogram showing the percent

volume of cement at different levels of stress for all loading conditions.[20] The average stress was found for each element, and then the elements were divided into groups with different stress levels. Spatial stress distributions were analyzed for transverse layers (Fig. 4.1).

The stress distribution and load transfer in the corrected OA scapula was compared to those in the healthy one. Since excessively retroverted glenoids are commonly returned to neutral version during TSA, comparing a corrected OA glenoid to a healthy glenoid minimized the variations induced by retroversion.

4.3 Results

4.3.1 Effect of Peg Proximity to Scapular Cortical Bone in Healthy and Osteoarthritic Shoulders

Load transfer in the healthy reconstructed shoulder was more sensitive to the proximity of the pegs to the cortex than that in the OA reconstructed shoulder. In the healthy reconstructed shoulder, the glenoid bone carried a higher percentage of the joint load when pegs did not touch the cortical bone (Fig. 4.3A). For longer pegs that touched the cortical bone, bone carried 67% of the joint load, whereas with shorter pegs that did not touch the cortical bone, the bone carried more than 73% of the load. This trend held for both center and posterior loading conditions. In the OA shoulders, regardless of retroversion angle, the load transfer pattern was less affected by peg lengths (Fig. 4.3B) for both center and posterior loading. The minimum percent load carried by the bone differed by <5% between retroversion angles.

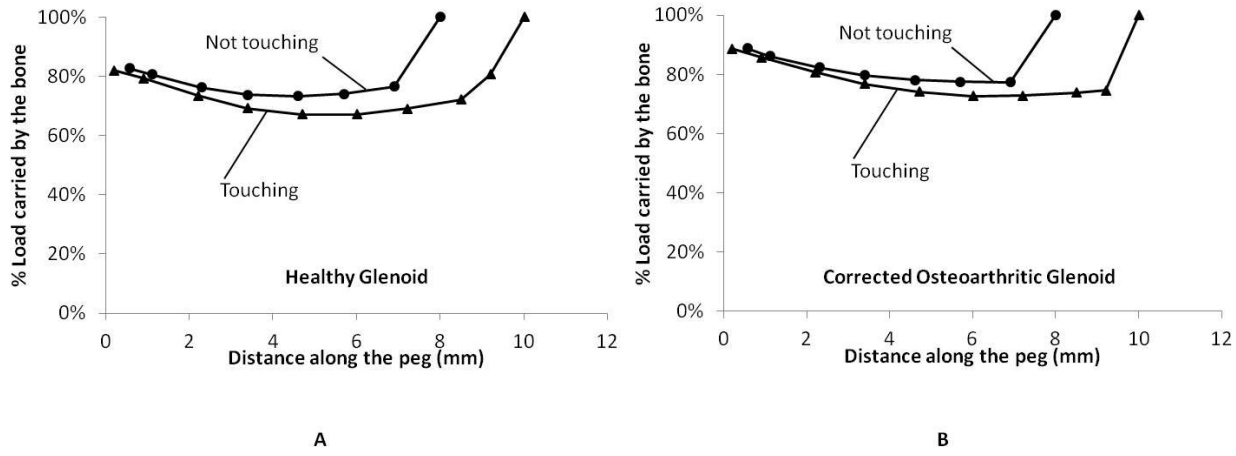

Figure 4.3 Percent load carried by the bone for center loading in healthy (A) and corrected (B) OA glenoids for the cases where the cemented pegs are touching and not touching the cortical bone. The cemented pegs begin at 0mm and end at 7mm and 9mm for the not touching and touching the cortical bone cases, respectively. The data points at 8mm and 10mm indicate the loading where no pegs are present for the not touching and touching the cortical bone cases, respectively.

4.3.2 Effect of Retroversion in Osteoarthritis: Retroverted vs. Corrected

Correcting for retroversion affected the ultimate load transfer pattern during posterior loading, but not for center loading (Figs. 4.4A and 4.4B). The bone in the corrected OA shoulder consistently carried less load than bone in the retroverted OA shoulder during posterior loading, regardless of whether the pegs were touching the cortical bone, as confirmed by the 10% increase in cement volume stressed between 2 and 4 MPa for a corrected OA glenoid compared to the retroverted glenoid during posterior loading (Fig. 4.5). Higher stresses occurred overall in the cement mantle for the corrected OA glenoid and in the bottom anterior peg when compared to the retroverted OA glenoid (Fig. 4.6).

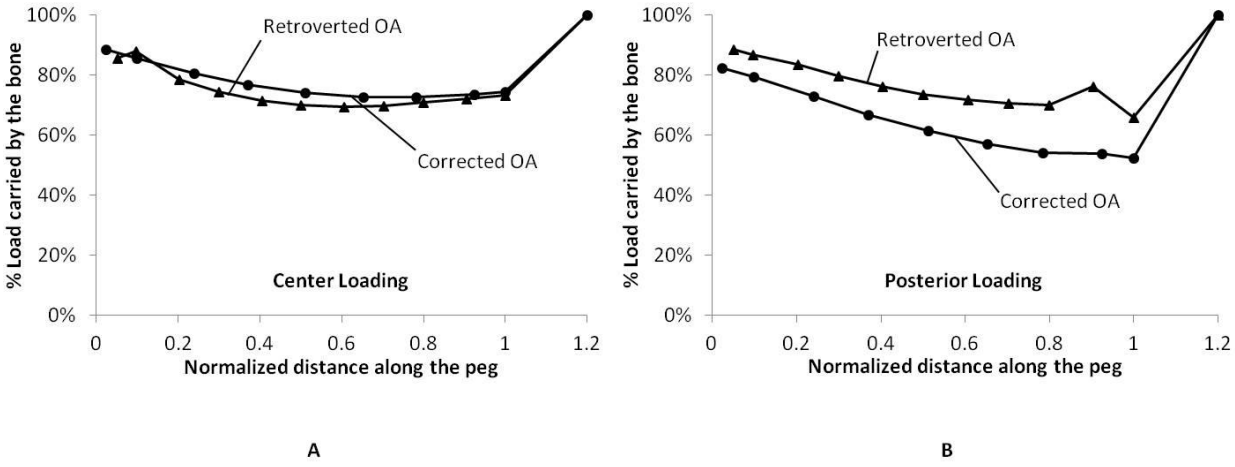

Figure 4.4 Percent load carried by the bone for center (A) and eccentric posterior (B) loading in the corrected and retroverted OA glenoids for the case where the cemented pegs are touching the cortical bone. Similar trends were determined regardless of whether the pegs were touching cortical bone. The x-axis represents the normalized length of the cemented pegs, where the pegs begin at 0 and end at 1. The data points at 1.2 indicate the loading where no pegs are present.

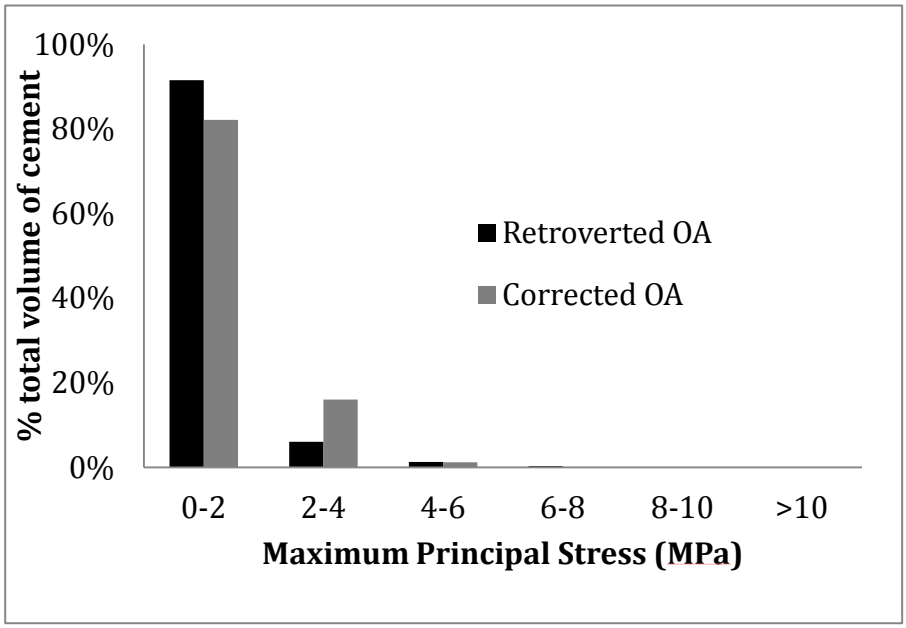

Figure 4.5 Maximum principal stress in the cement layer during eccentric posterior loading for the case where implant pegs are touching the cortical bone in the corrected and retroverted OA glenoids.

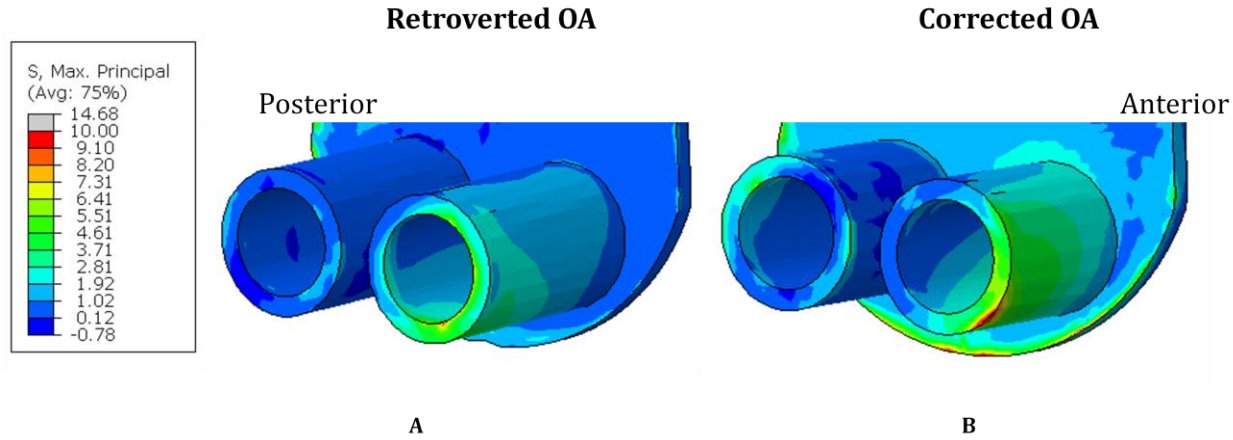

Figure 4.6 A posterior view of the maximum principal stress distributions in the cement layer for eccentric posterior loading. Zoomed into the anterior and posterior inferior pegs for the retroverted and corrected OA glenoids for the case where the implant pegs are touching the cortical bone.

4.3.3 Effect of Eccentric Loading in Healthy and Osteoarthritic Shoulders

Eccentric loading on the glenohumeral joint had little effect on load transfer patterns in the retroverted OA glenoid regardless of whether the pegs were touching cortical bone (Fig. 4.7A). However, when the retroversion was corrected, the load carried by the bone was significantly less during posterior loading compared to center loading, again regardless of whether the pegs were touching the cortical bone (differences ranged between 7 and 22%, as shown in Fig. 4.7B). This is confirmed by the 16% increase in cement volume stressed between 2 and 6 MPa during posterior loading (Fig. 4.8). Stress distributions in the cement layer showed the increase in maximum tensile stresses during posterior loading compared to center loading in the corrected OA shoulder (Fig. 4.9); no such observations were seen in the retroverted OA shoulder.

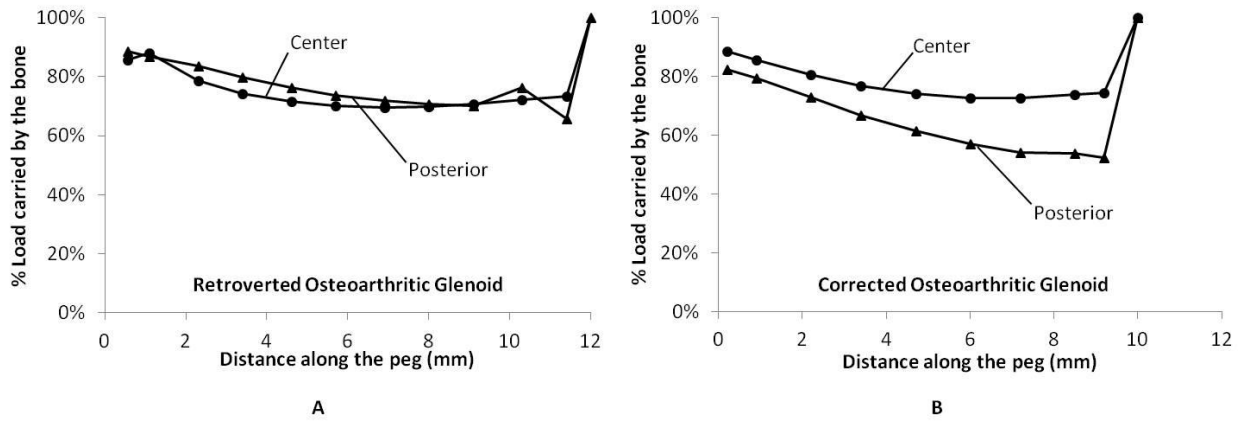

Figure 4.7 Percent load carried by the bone for center and eccentric posterior loading for the retroverted (A) and corrected (B) OA glenoids for the case of the implant pegs touching the cortical bone. Similar trends were determined regardless of whether the pegs were touching cortical bone. The cemented pegs begin at 0mm and end at 9mm. The data point at 10mm indicates the loading where no pegs are present.

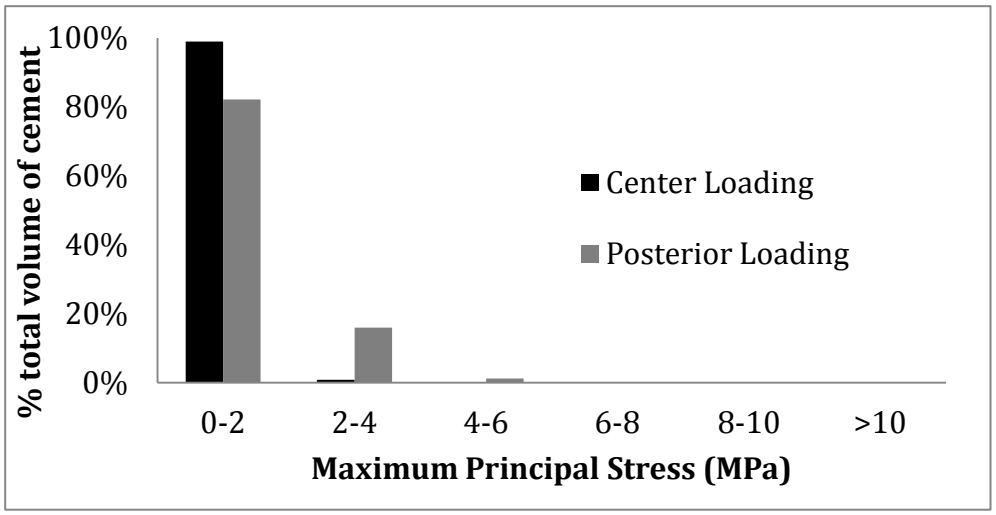

Figure 4.8 Maximum principal stress in the cement layer during center and eccentric posterior loading in the corrected OA glenoid for the case where implant pegs are touching the cortical bone.

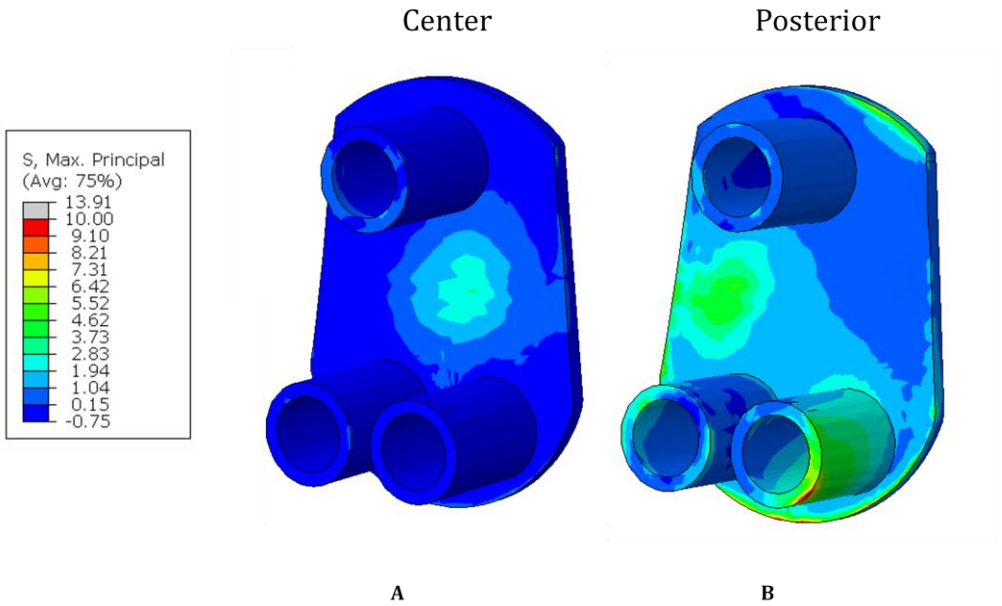

Figure 4.9 A posterior view of the maximum principal stress distributions in the cement layer during center and posterior loading in the corrected osteoarthritic glenoid for the case where implant pegs are touching the cortical bone.

The differences in load carried by the bone in the healthy glenoid were less significant between center and posterior loading, regardless of whether the pegs were touching the cortical bone when compared to the corrected OA glenoid. During center loading, the glenoid bone in the corrected OA shoulder carried a higher percentage of the load than the healthy glenoid; however, with posterior loading the load carried by the OA bone dropped to less than that of the healthy bone (Fig. 4.10).

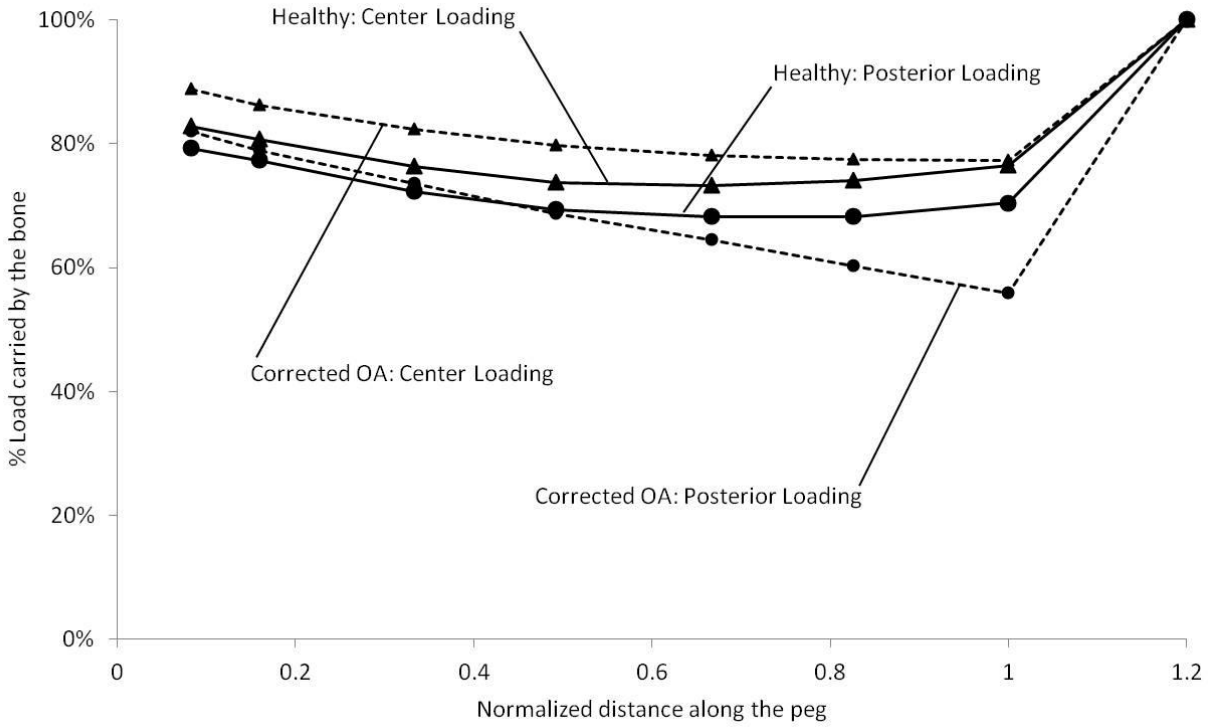

Figure 4.10 Percent load carried by the bone during center and eccentric posterior loading in the healthy and corrected OA glenoids for the case where the implant pegs are away from the cortical bone. The x-axis represents the normalized length of the cemented pegs, where the pegs begin at 0 and end at 1. The data points at 1.2 indicate the loading where no pegs are present.

4.4 Discussion

We sought to understand the effects of osteoarthritis-induced changes in bone density and retroversion angle of the scapula on load transfer and stress distribution in the bone-implant system of a TSA. We developed finite element models of both a healthy and osteoarthritic reconstructed scapula implanted with a contemporary glenoid component, and determined the stress distributions and load transfer in healthy, corrected and retroverted osteoarthritic scapulas during eccentric loading.

In answer to our first research question, we found that peg proximity to the cortical shell had a larger effect on load transfer in the healthy glenoid than in the OA glenoids. In the healthy

glenoid, as peg length decreased, the glenoid bone carried a higher percent of the total joint load (Fig. 4.3A). When the peg is touching the cortical shell, the joint load is directly transferred from the implant to the stiff outer cortical bone at the end of the peg. This results in load bypassing the middle cancellous bone region and decreasing the load carried by the bone. From a mechanical standpoint, longer pegs (as in the case with a peg that is touching the cortical bone) have more shear stress acting along its length.[9] The outcome of higher shear stress is more frictional force between the bone and the implant that resists the motion of the peg. Higher frictional force causes less deformation, and therefore, lowers normal strain in the bone, which results in less load carried by the bone for implants with longer pegs. OA bone is stiffer than healthy bone.[4,5,12,24] Therefore, the stiffer surrounding cancellous bone is able to take more joint load even when the peg is touching the cortical shell. To explain this result mechanically, it is necessary to understand how bone density plays a role on the shear stress in addition to the peg length. According to mechanics of a composite material, when the stiffness of the surrounding material increases, the effect of peg length on the shear stress in that material decreases.[15] Therefore, a reduction in peg length in the stiffer OA bone resulted in a smaller change of strain in the bone. Thus, a smaller change in load carried by the bone is expected. Surgically, this observation highlights that OA patients can accommodate shorter pegs since OA glenoids are less sensitive to the proximity of the end of the peg to the cortical bone. Shorter pegs would allow for less bone resection and reduce the chance that a peg could perforate the cortex in smaller patients.

Surprisingly, in answer to our second question, we demonstrated that correcting for retroversion in OA glenoids may actually increase the risk for stress shielding and cement failure compared to retroverted glenoids. Our results showed that during center loading, the load

transfer patterns in the corrected and retroverted OA glenoids were similar (Fig. 4.4A); however, with posterior loading, the load carried by bone in the corrected OA glenoid decreased significantly (Fig. 4.4B). This decrease can be understood by realizing that to correct the retroversion, a considerable amount of bone on the anterior side of the glenoid must be reamed to return the version angle after TSA closer to 0°.[26] This causes a change in placement of the implant pegs within the glenoids, and as a result, the implant pegs are fixed in bone regions with different stiffnesses (Fig. 4.11). In the retroverted glenoid, little bone was removed to accommodate the implant whereas in the corrected glenoid, the anterior surface was significantly reamed to recreate the neutral version angle resulting in the removal of stiff anterior bone. Therefore, for the retroverted OA glenoid, both inferior pegs were inserted into stiffer bone, while in the corrected OA glenoid, the anterior inferior peg was fixed in less stiff bone compared to the posterior peg (Fig. 4.11).

The cement layer in the corrected OA glenoid must carry higher tensile stresses than the cement layer in the retroverted glenoid, causing lower percent joint load carried in the corrected OA glenoid bone (Figs. 4.4B and 4.5). Furthermore, higher tensile stresses were observed in the cement surrounding the inferior anterior peg of the corrected OA glenoid compared to the retroverted OA glenoid (Fig. 4.6). Thus, in the corrected OA case, the bone may be prone to stress shielding and the cement to mechanical failure at higher eccentric loads. These results suggest that the current surgical practice of correcting retroversion may not be beneficial in improving implant fixation. This also supports the current surgical trend towards minimal glenoid reaming in order to preserve subcortical bone to improve implant stability.

The presumed purpose of correcting retroversion is to minimize posterior subluxation, thereby mitigating the rocking horse phenomenon.[26] Interestingly, we found that the load transfer

pattern and cement stresses in the retroverted OA glenoid were less affected by loading location than in the corrected OA glenoid. The load transfer patterns in the retroverted OA glenoid were similar between center and posterior loading (Fig. 4.7A), while the corrected OA glenoid was more sensitive to changes in loading location with a significant decrease in the amount of load carried by the bone during posterior loading (Fig. 4.7B), and an increase in the volume of highly stressed cement (Figs. 4.8 and 4.9). This is most likely due to the removal of stiff anterior bone when reaming the glenoid to its neutral retroversion angle. Because the anterior bottom peg was fixed in less stiff bone while the posterior bottom peg was fixed in more stiff bone (Fig. 4.11), the posterior side of the implant is better fixed. Thus, when posterior forces are applied to the implant, the cement on the anterior (weaker) quadrant is subject to high tensile stresses (Fig. 4.9). This suggests that glenoid loosening due to cement or bone-cement interface failure is a likely scenario in a corrected OA glenoid especially at higher loads.

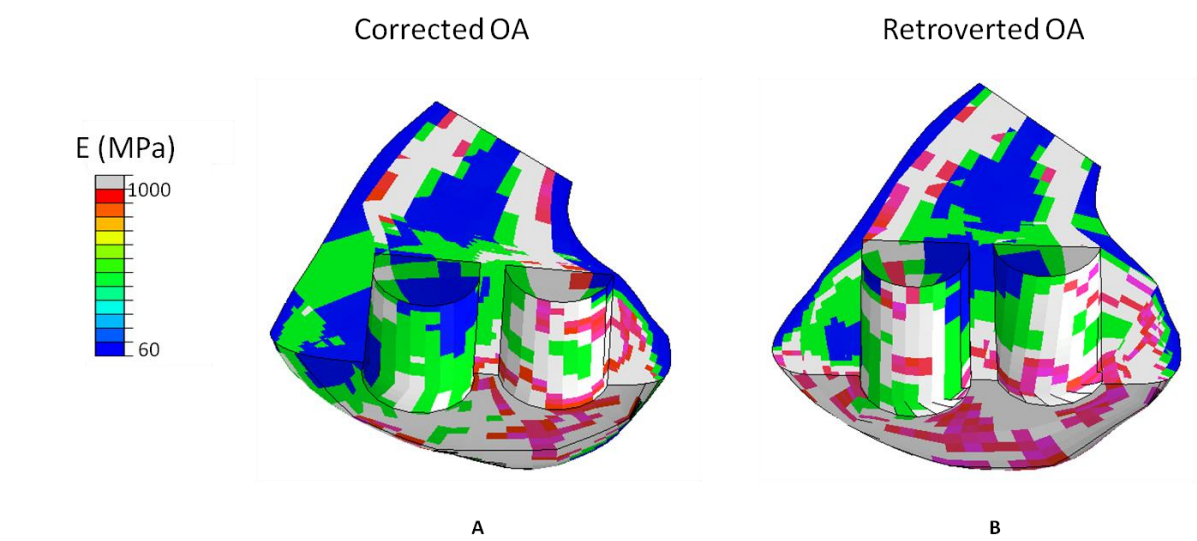

Figure 4.11 Superior views of transverse cross-sections of elastic modulus (stiffness) distributions in the corrected (A) and retroverted (B) OA glenoids in the inferior pegs for the case where the cemented pegs are touching the cortical bone. Areas of gray represent bone regions of high stiffness.

Our results suggested that when eccentric posterior loading occurs on the corrected OA, it may be more prone to stress shielding and cement failure than the healthy glenoid. When comparing the load transfer patterns between the healthy and corrected OA glenoids, the corrected OA glenoid was more sensitive to eccentric loading than in the healthy (Fig. 4.10). Compared to the healthy glenoid, the corrected OA patient bone stiffness increased, and the anterior region is less stiff than the posterior region.[4,5,12,24] When changing from center to posterior loading, the cement in the OA glenoid experiences a larger increase in tensile stresses in the cement than in the cement in the healthy glenoid.

Our study has limitations. We used CT scan data from one healthy and one OA subject, so our results should be interpreted in terms of the general effects of introduction of an implant in a healthy and diseased (OA) environment, of physiological alterations in the location of the joint load on the glenoid, and of glenoid retroversion. Although high similarities in geometry (shape) and bone density distribution were observed among the three OA shoulders that we CT-scanned, anatomical variables, such as glenoid size, version, and inclination, may still be different among individuals. These variables affect the resulting FE mesh, which in turn influences the calculated stresses. The bone was modeled as linear elastic, but this was a reasonable assumption since the bone tissue in the models never experienced stresses beyond the tissue's yield stress. Also, we assumed fully bonded interfaces representative of a well-functioning TSA. If this assumption were relaxed, we would expect higher stresses at the interfaces, especially during eccentric loading. Similarly, we assumed an even 1mm layer of cement around the implant, which may be difficult to achieve surgically. Finally, although we present the bone density distributions for one OA glenoid, we analyzed three glenoids to confirm

that overall stiffness increased with OA. This is further buttressed by a CT study of glenoids and other bone density studies.[4,5,12,24]

4.5 Conclusion

In conclusion, we provided evidence of how load sharing is altered among healthy and corrected and retroverted OA glenoids. Our results suggest that with reconstruction of the corrected glenoid with a contemporary implant, the load transfer pattern changes with eccentric loads increasing stresses in the cement. The load transfer and local stresses in the bone-implant system in the retroverted glenoid is less sensitive to changes in loading location. Furthermore, due to lower glenoid bone stiffness in the healthy glenoid, the load transfer in the OA glenoids is less sensitive to the effect of peg proximity to the cortical shell than in the healthy glenoid.

REFERENCES

1. Bohsali KI, Wirth MA, Rockwood CA. Complications of total shoulder arthroplasty. J Bone Joint Surg Am. 2006;88(10):2279–92. doi:10.2106/JBJS.F.00125

2. Bryce CD, Davison AC, Okita N, Lewis GS, Sharkey NA, Armstrong AD. A biomechanical study of posterior glenoid bone loss and humeral head translation. J Shoulder Elbow Surg. 2010;19(7):994–1002. doi: 10.1016/j.jse.2010.04.010

3. Couteau B, Mansat P, Estivalèzes E, Darmana R, Mansat M, Egan J. Finite element analysis of the mechanical behavior of a scapula implanted with a glenoid prosthesis. Clin Biomech. 2001;16(7):566–75.

4. Couteau B, Mansat P, Mansat M, Darmana R, Egan J. In vivo characterization of glenoid with use of computed tomography. J Shoulder Elbow Surg. 2001;10(2):116–22. doi:10.1067/mse.2001.112884

5. Dequeker J, Mokassa L, Aerssens J, Boonen S. Bone density and local growth factors in generalized osteoarthritis. Microsc Res Tech. 1997;37(4):358–71. doi:10.1002/(SICI)1097-0029(19970515)37:4<358::AID-JEMT10>3.0.CO;2-L

6. Farron A, Terrier A, Büchler P. Risks of loosening of a prosthetic glenoid implanted in retroversion. J Shoulder Elbow Surg. 2006;15(4):521–6. doi:10.1016/j.jse.2005.10.003

7. Franklin JL, Barrett WP, Jackins SE, Matsen FA. Glenoid loosening in total shoulder arthroplasty. Association with rotator cuff deficiency. J Arthroplasty. 1988;3(1):39–46.

8. Frich H, Jensen NC, Odgaard A, Pedersen CM, Sojbjerg JO, Dalstra M. Bone strength of the glenoid and material properties. J Shoulder Elbow Surg. 1997;6(2):97–1104.

9. Giori NJ, Beaupré GS, Carter DR. The influence of fixation peg design on the shear stability of prosthetic implants. J Orthop Res. 1990;8(6):892–8. doi:10.1002/jor.1100080615

10. Gupta S, Van der Helm FCT, Van Keulen F. The possibilities of uncemented glenoid component--a finite element study. Clin Biomech. 2004;19(3):292–302. doi:10.1016/j.clinbiomech.2003.12.002

11. Gupta S, Van der Helm FCT. Load transfer across the scapula during humeral abduction. J Biomech. 2004;37(7):1001–9. doi:10.1016/j.jbiomech.2003.11.025

12. Hart DJ, Cronin C, Daniels M, Worthy T, Doyle D V, Spector TD. The Relationship of Bone Density and Fracture to Incident and Progressive Radiographic Osteoarthritis of the Knee The Chingford Study. Arthritis Rhem. 2002;46(1):92–99. doi:10.1002/art.10057

13. Hertel R, Ballmer FT. Observations on retrieved glenoid components. J Arthroplasty. 2003;18(3):361–6. doi:10.1054/arth.2003.50048

14. Hill JM, Norris TR. Long-term results of total shoulder arthroplasty following bone-grafting of the glenoid. J Bone Joint Surg Am. 2001;83-A(6):877–83.

15. Hull D, Clyne TW. An Introduction to Composite Material. New York: Cambridge University Press; 1981.

16. Hvid I, Bentzen SM, Linde F, Mosekilde L, Pongsoipetch B. X-ray quantitative computed tomography: the relations to physical properties of proximal tibial trabecular bone specimens. J Biomech. 1989;22(8-9):837–44.

17. Iannotti JP, Norris T. Influence of Preoperative Factors on Outcome of Shoulder Arthroplasty for Glenohumeral Osteoarthritis. J Bone Joint Surg. 2003;85-A(2):251–258.

18. Junaid S, Gupta S, Sanghavi S, Anglin C, Roger E, Amis A, et al. Failure mechanism of the all-polyethylene glenoid implant. J Biomech. 2010;43(4):714–9. doi:10.1016/j.jbiomech.2009.10.019

19. Lacroix D, Murphy LA, Prendergast PJ. Three-dimensional finite element analysis of glenoid replacement prostheses: a comparison of keeled and pegged anchorage systems. J Biomech Eng. 2000;122(4):430–6.

20. Lennon A, Prendergast PJ. Evaluation of cement stresses in finite element analyses of cemented orthopaedic implants. J Biomech Eng. 2001;123(6):623–628.

21. Mansat P, Barea C, Hobatho M-C, Darmana R, Mansat M. Anatomic variation the glenoid of the mechanical properties of the glenoid. J Shoulder Elbow Surg. 1998;7(2):109–115.

22. Mansat P, Briot J, Mansat M, Swider P. Evaluation of the glenoid implant survival using a biomechanical finite element analysis: influence of the implant design, bone properties, and loading location. J Shoulder Elbow Surg. 2007;16(3):S79–S83. doi:10.1016/j.jse.2005.11.010

23. Massimini DF, Li G, Warner JP. Glenohumeral contact kinematics in patients after total shoulder arthroplasty. J Bone Joint Surg Am. 2010;92(4):916–26. doi:10.2106/JBJS.H.01610

24. Nevitt MC, Lane NE, Scott JC, Hochberg MC, Pressman AR, Genant HK, et al. Radiographic osteoarthritis of the hip and bone mineral density. The study of osteoporotic fractures research group. Arthritis Rheum.1995;38(7):907–916.

25. Nho SJ, Nam D, Ala OL, Craig E V, Warren RF, Wright TM. Observations on retrieved glenoid components from total shoulder arthroplasty. J Shoulder Elbow Surg. 2009;18(3):371–378. doi:10.1016/j.jse.2008.12.006

26. Nowak DD, Bahu MJ, Gardner TR, Dyrszka MD, Levine WN, Bigliani LU, et al. Simulation of surgical glenoid resurfacing using three-dimensional computed tomography of the arthritic glenohumeral joint: the amount of glenoid retroversion that can be corrected. J Shoulder Elbow Surg. 2009;18(5):680–8. doi:10.1016/j.jse.2009.03.019

27. Nuttall D, Haines JF, Trail II. A study of the micromovement of pegged and keeled glenoid components compared using radiostereometric analysis. J Shoulder Elbow Surg. 2004;16(3):S65–70. doi:10.1016/j.jse.2006.01.015

28. Patel R, Wright T, Gao Y. Load Transfer after Cemented Total Shoulder Arthroplasty. Journal of Shoulder and Elbow Surgery. 2014 (Accepted)

29. Rice JC, Cowin SC, Bowman JA. On the dependence of the elasticity and strength of cancellous bone on apparent density. J Biomech. 1988;21(2):155–68.

30. Schaffler MB, Burr DB. Stiffness of compact bone: effects of porosity and density. J Biomech. 1988;21(1):13–6.

31. Skirving AP. Total shoulder arthroplasty -- current problems and possible solutions. J Orthop Sci. 1999;4(1):42–53.

32. Soslowsky LJ, Flatow EL, Bigliani LU, Pawluk RJ, Ateshian GA, Mow VC. Quantitation of in situ contact areas at the glenohumeral joint: a biomechanical study. J Orthop Res. 1992;10(4):524–34. doi:10.1002/jor.1100100407

33. Strauss EJ, Roche C, Flurin P-H, Wright T, Zuckerman JD. The glenoid in shoulder arthroplasty. J Shoulder Elbow Surg. 2009;18(5):819–33. doi:10.1016/j.jse.2009.05.008

34. Terrier A, Büchler P, Farron A. Bone-cement interface of the glenoid component: stress analysis for varying cement thickness. Clin Biomech. 2005;20(7):710–7. doi:10.1016/j.clinbiomech.2005.03.010

35. Terrier A, Büchler P, Farron A. Influence of glenohumeral conformity on glenoid stresses after total shoulder arthroplasty. J Shoulder Elbow Surg. 2006;15(4):515–20. doi:10.1016/j.jse.2005.09.021

36. Veeger HEJ, Van der Helm FCT. Shoulder function: the perfect compromise between mobility and stability. J Biomech. 2007;40(10):2119–29. doi:10.1016/j.jbiomech.2006.10.016

37. Wirth MA, Rockwood CA. Current Concepts Review - Complications of Total Current Concepts Review Complications of Total Shoulder-Replacement Arthroplasty. J Bone Joint Surg Am. 1996;78(4):603–16.

38. Yian EH, Werner CML, Nyffeler RW, Pfirrmann CW, Ramappa A, Sukthankar A, et al. Radiographic and computed tomography analysis of cemented pegged polyethylene glenoid components in total shoulder replacement. J Bone Joint Surg Am. 2005;87(9):1928–36. doi:10.2106/JBJS.D.02675

Chapter 5

Conclusions and Future Directions

5.1 Summary and Conclusions

The overarching goal of this thesis was to establish an understanding of the kinematics and mechanics of the reconstructed glenohumeral joint. The results indicate posterior glenohumeral translation after an unconstrained total shoulder arthroplasty (TSA) due to muscle activation of the infraspinatus, potential for stress shielding of the cancellous bone in the healthy glenoid after TSA, and a higher possibility of stress shielding and cement failure in the corrected osteoarthritic glenoid compared to the retroverted osteoarthritic and healthy glenoids after a TSA.

The objective of Chapter 2 was to explain the posterior glenohumeral translations observed clinically. A six degree of freedom computational model of the shoulder joint was developed to explain clinical observations of posterior translation. The model took inputs of glenohumeral geometry, used a physiological optimization criterion to determine the necessary muscle forces required to maintain contact between the humeral head and glenoid surfaces while reaching the scaption angle of interest, and output the resulting joint contact force magnitude and location. Radial mismatches between 1 and 20mm of the humeral head and glenoid implants were simulated. This study determined that posterior translation increased as a function of radial

mismatch. The increase in posterior translation was explained by the increase in muscle force in the infraspinatus muscle. Although individual muscle forces changed, the joint contact force magnitude and location remained relatively constant for all radial mismatches. The translation of the humeral head on the glenoid for various radial mismatches agreed with clinical observations of posterior translation.

The focus of Chapter 3 was to gain an understanding of the load transfer through the glenoid before and after reconstruction. Our aim was to determine how load transfer and stress distribution were affected by the introduction of a glenoid implant, by physiological alterations in the location and magnitude of the joint load on the glenoid, and by the presence of a metal-backing. A finite element model was developed to understand how the joint load applied at the surface of the implant is carried through the bone-implant system. A metal-backed glenoid component was also simulated to understand the effects of a stiffer fixation layer. This study determined after a cemented TSA, stress shielding was possible because load bypassed the cancellous bone region and was transferred directly to the stiff cortical bone when the implant pegs were present. Additionally, the cement was more likely to failure during eccentric and high magnitude loading. The metal-backed implant showed a significant decrease in load carried by the bone compared to the cemented implant which confirmed clinical observations of stress-shielding and loosening in these implants.

The aim of Chapter 4 was to understand the effects of osteoarthritis induced changes in bone density and retroversion angle of the scapular on load transfer and stress distribution in the bone-implant system of scapula. Chapter 4 incorporated the effects of the osteoarthritic glenoid after a TSA during eccentric loading. Finite element models were developed of both a healthy and osteoarthritic reconstructed scapula implanted with a contemporary glenoid component.

Results showed that stress shielding was more likely in the corrected osteoarthritic glenoid compared to the healthy and retroverted osteoarthritic glenoids. Additionally, the osteoarthritic glenoid was more sensitive to eccentric loading than the retroverted and healthy glenoids. A higher percent of the cement volume was stressed between 2 and 4 MPa, and less joint load was carried by the glenoid bone during eccentric loading in the corrected osteoarthritic glenoid. These findings question the common surgical practice of correcting for glenoid retroversion prior to reconstruction. Furthermore, our results determined that the reconstructed osteoarthritic glenoid was less sensitive to peg proximity to the scapular shell than the healthy glenoid. This was due to the increase in stiffness that occurs in osteoarthritic patients. This finding demonstrates that shorter pegs requiring less bone resection may be used in osteoarthritic patients.

Contemporary total shoulder replacements are successful in the short and mid-term, however the failure rate is high in the long-term due to glenoid component loosening. The long-term goal is to design a total shoulder implant system that can withstand the eccentric loading that commonly occurs in the glenohumeral joint. However to design such a system requires knowledge of how the kinematics and mechanics of the joint are altered after reconstruction in order to identify potential areas for failure. The computational model of the shoulder joint and the finite element models developed in this thesis approached understanding the kinematics and mechanics of the joint differently from previous studies by determining the muscle activations and glenohumeral translations in a six degree of freedom joint and the load transfer pathways in the bone-implant systems of healthy and osteoarthritic joints. In the short-term this information may be applied to improve current surgical operation procedures and post-operative rehabilitation techniques, and in the long term, to design implants that prevent stress shielding,

decrease tensile stresses in the fixation layer, and can withstand the effects of eccentric loading at the fixation-bone interface.

Towards these goals, it will be beneficial to preserve the stiff anterior glenoid bone during the reaming procedure so that the implant pegs are fixed in stiff bone both on the anterior and posterior sides. Instead of the current recommendation to ream the anterior bone all the way back to neutral version, perhaps the protocol should ream enough to reduce possibility of posterior dislocation so that some anterior stiff bone is preserved. Stiffer bone surrounding the implant will increase the likelihood that the joint load will transfer from the cemented implant pegs to the cancellous bone region. Furthermore, shorter implant pegs may allow for the load to transfer sooner to the cancellous bone. However, future studies will have to investigate the effect of shorter peg lengths on generating tensile stresses in the cement and at the bone-cement interface. The results from this research also suggest that the fixation material is at risk of failure due to its brittle nature so designing a more compliant material for fixation will more closely mimic the mechanics of the articulating cartilage and allow for eccentric loading to occur while decreasing the probability of failure due to tensile stresses.

5.2 Future Directions

With the conclusion of the studies in this thesis, we realize a number of questions are raised and specific research areas are identified that may be pursued in more detail. Using the six degree of freedom shoulder model and finite element models, several important studies may be conducted regarding the kinematics and mechanics of the native glenohumeral joint and after a TSA: 1) an understanding of the kinematics of the joint due to retroversion, 2) an

understanding of joint mechanics and load transfer when cement is de-bonded from bone, and 3) finite element analysis of a larger number of healthy and osteoarthritic scapulas to understand bone density changes within a larger population.

First, TSAs are typically performed in osteoarthritic patients that most likely will have some degree of retroversion. Through the use of both the physical shoulder simulator and the six degree of freedom computational shoulder model, multiple models of glenohumeral joints may be generated to understand the effects of retroversion on muscle activation, joint contact force and translation. Results from these studies may be used to better direct physical rehabilitation post-operatively and strengthen muscles observed to be important in maintaining stability.

Secondly, the current finite element models provide a basic understanding of mechanics in the bone-implant system under an ideal assumption that the cement layer is fully bonded to the bone. In a more realistic environment, there would be a frictional interface between the bone and cement surfaces. Micro-motion may be present during daily activities of living resulting in debonding. Future studies should understand the effects of cement debonding on load transfer and cement layer stresses. Debonding coupled with eccentric loading may certainly affect the load transfer more extremely than observed during a fully-bonded case. Therefore, more complex finite element models are needed to simulate realistic conditions in order to better explain clinical observations of glenoid component loosening and failure.

Finally, the conclusions drawn from the current finite element studies were based on one healthy and one osteoarthritic scapula. Due to the time-investment of creating high-grade meshes of complex geometries of the scapula, multiple finite element models were not created in the time span of this thesis. Future studies should be directed towards understanding the load transfer in numerous bone models. Osteoarthritis is associated with changes in the spatial density of

glenoid bone, and only one study to date has quantified this effect. It is imperative to understand the effects of osteoarthritis in a larger population in order to determine how implant fixation may be affected as a result.